Journal of
METAMORPHIC GEOLOGY

J. metamorphic Geol., 2013, **31**, 585–606 doi:10.1111/jmg.12034

Neotethys closure history of Anatolia: insights from ^{40}Ar–^{39}Ar geochronology and *P–T* estimation in high-pressure metasedimentary rocks

A. POURTEAU,[1] M. SUDO,[1] O. CANDAN,[2] P. LANARI,[3] O. VIDAL[3] AND R. OBERHÄNSLI[1]
[1]*Institut für Erd- und Umweltwissenschaften, Universität Potsdam, Karl–Liebknecht–Straße 24–25, Potsdam–Golm, 14476, Germany (pourteau@geo.uni-potsdam.de)*
[2]*Dokuz Eylül Üniversitesi, Mühendislik Fakültesi, Jeoloji Mühendisliği Bölümü, Tınaztepe Kampusu, Buca–Izmir, 35160, Turkey*
[3]*Isterre, Université Joseph Fourier Grenoble, CNRS, 1381 rue de la Piscine, Grenoble Cedex 09, 38041, France*

ABSTRACT The multiple high-pressure (H*P*), low-temperature (L*T*) metamorphic units of Western and Central Anatolia offer a great opportunity to investigate the subduction- and continental accretion-related evolution of the eastern limb of the long-lived Aegean subduction system. Recent reports of the H*P*–L*T* index mineral Fe-Mg-carpholite in three metasedimentary units of the Gondwana-derived Anatolide–Tauride continental block (namely the Afyon Zone, the Ören Unit and the southern Menderes Massif) suggest a more complicated scenario than the single-continental accretion model generally put forward in previous studies. This study presents the first isotopic dates (white mica ^{40}Ar–^{39}Ar geochronology), and where possible are combined with *P–T* estimates (chlorite thermometry, phengite barometry, multi-equilibrium thermobarometry), on carpholite-bearing rocks from these three H*P*–L*T* metasedimentary units. It is shown that, in the Afyon Zone, carpholite-bearing assemblages were retrogressed through greenschist-facies conditions at *c.* 67–62 Ma. Early retrograde stages in the Ören Unit are dated to 63–59 Ma. In the Kurudere–Nebiler Unit (H*P* Mesozoic cover of the southern Menderes Massif), H*P* retrograde stages are dated to *c.* 45 Ma, and post-collisional cooling to *c.* 26 Ma. These new results support that the Ören Unit represents the westernmost continuation of the Afyon Zone, whereas the Kurudere–Nebiler Unit correlates with the Cycladic Blueschist Unit of the Aegean Domain. In Western Anatolia, three successive H*P*–L*T* metamorphic belts thus formed: the northernmost Tavşanlı Zone (*c.* 88–82 Ma), the Ören–Afyon Zone (between 70 and 65 Ma), and the Kurudere–Nebiler Unit (*c.* 52–45 Ma). The southward younging trend of the H*P*–L*T* metamorphism from the upper and internal to the deeper and more external structural units, as in the Aegean Domain, points to the persistence of subduction in Western Anatolia between 93–90 and *c.* 35 Ma. After the accretion of the Menderes–Tauride terrane, in Eocene times, subduction stopped, leading to continental collision and associated Barrovian-type metamorphism. Because, by contrast, the Aegean subduction did remain active due to slab roll-back and trench migration, the eastern limb (below Southwestern Anatolia) of the Hellenic slab was dramatically curved and consequently teared. It therefore is suggested that the possibility for subduction to continue after the accretion of buoyant (e.g. continental) terranes probably depends much on palaeogeography.

Key words: ^{40}Ar–^{39}Ar geochronology; Anatolia; chlorite–phengite thermobarometry; high-pressure metasedimentary rocks.

INTRODUCTION

The Mediterranean realm represents one of the greatest natural laboratories for investigating subduction- and continental accretion-related geodynamics. The integration of multi-disciplinary data has demonstrated that, due to subduction retreat, subduction of a single lithospheric slab could persist despite the accretion of buoyant micro-continental terranes to the trench (e.g. Malinverno & Ryan, 1986; Royden & Burchfiel, 1989; Jolivet & Faccenna, 2000; van Hinsbergen *et al.*, 2005). This phenomenon, recognized in several other subduction systems worldwide, like the Scotia–Sandwich, the Lesser Antilles and the Banda subduction zones, results in concave trenches and 'spoon-shaped' down-going slabs (Hsui & Youngquist, 1985; Spakman & Hall, 2010), which in general are delimited laterally by sub-vertical slab tears, expressed, at the surface, by strike-slip faulting and specific volcanic activity (Govers & Wortel, 2005). Slab roll-back, trench migration and -curving, and slab tearing, also reproduced by analogue and numerical modelling experiments (e.g. Husson *et al.*, 2009; Schellart, 2010), are processes commonly envisaged for the evolution of retreating subduction systems. However, what controls the location and timing of lateral disruption is not fully resolved, as in the Aegean Domain in particular.

In the Aegean subduction system, the retreat of the Hellenic NW- to NE-plunging slab is notably illustrated by the younging, from the inner to the outer parts of the upper plate, of extensional tectonics, arc magmatic activity and high-pressure (H*P*), low-temperature (L*T*) metamorphic events (e.g. Ring *et al.*, 2010; Jolivet *et al.*, 2013). According to a generally accepted model, in response to the burial of continental terranes, subduction temporarily stalled, then the slab rolled back, and the accreted crustal terranes were decoupled from the underlying, down-going lithosphere leading to trench migration towards the foreland (Jolivet & Faccenna, 2000; van Hinsbergen *et al.*, 2005; Jolivet & Brun, 2008). As displayed on tomographic images, the Hellenic slab is interrupted to the east by a slab tear located below Southwestern Anatolia (Bijwaard *et al.*, 1998; Biryol *et al.*, 2011; Salaün *et al.*, 2012). According to its possible volcanic expression in Western Anatolia, this tear might have formed at *c.* 20 Ma (Dilek & Altunkaynak, 2009). However, the understanding of the evolution of subduction at the eastern periphery of the Aegean Domain lacks accurate temporal constraints on continental-accretion events. Therefore, to gain insights into the disruption of the Hellenic slab, the evolution of the multiple H*P*–L*T* metamorphic units exposed in Western and Central Anatolia was investigated.

In Western and Central Anatolia, subduction- and collision-related metamorphic events associated with the accretion of the Gondwana-derived Anatolide–Tauride Block to the southern composite margin of Eurasia occurred in an interval greater than 40 Ma—88–82 Ma for the H*P*–L*T* metamorphism *v.* likely 45–30 Ma for the Barrovian metamorphism (see details below). For comparison, in other collisional belts, subduction-related metamorphism is followed by a collision-related overprint within 15–20 Ma or less (e.g. Western Himalaya, de Sigoyer *et al.*, 2000; Armenia, Rolland *et al.*, 2009; Central Alps, Wiederkehr *et al.*, 2009; Southeastern Turkey, Oberhänsli *et al.*, 2012). Although this peculiar timing was documented for more than a decade (Sherlock *et al.*, 1999), no tectonic reconstruction for Anatolia accounts for this peculiar feature yet.

In the past few years, Fe-Mg-carpholite-bearing assemblages, as evidence for H*P*–L*T* metamorphism, were documented in several tectonic units of Western and Central Anatolia (Oberhänsli *et al.*, 2001; Rimmelé *et al.*, 2003a,b, 2006; Candan *et al.*, 2005; Pourteau *et al.*, 2010) that were until then supposedly characterized by greenschist-facies metamorphism (e.g. Okay *et al.*, 1996). These discoveries, although shattering previous geodynamic reconstructions, have opened perspectives towards a better understanding of the subduction- and collision accretion-related tectonics in this region. To place their burial and exhumation into an accurate timeframe, the timing of subduction-related metamorphism in these units still needs to be determined. In consequence, this study combines ^{40}Ar–^{39}Ar geochronology and, when possible, thermobarometric calculations in white mica-, carpholite-bearing rocks and uses these results to discuss the significance of the isotopic dates. Based on these new data, a new evolutionary model for Western and Central Anatolia from *c.* 85 Ma to the present situation is proposed.

GEOLOGICAL SETTINGS

Tectonic domains of Western Anatolia

Western to Central Anatolia is composed of three tectonic regions that experienced contrasting tectonic histories between the Late Cretaceous and Palaeogene (Ketin, 1966). Northern Anatolia exposes a polystage fold-thrust belt known as the Pontides, which are characterized by pre-Jurassic metamorphic rocks with unconformable non-metamorphosed Jurassic to Cretaceous sedimentary and volcanic rocks (Altiner *et al.*, 1991; Yılmaz *et al.*, 1995; Okay & Sahinturk, 1997). Central Anatolia is composed of the Central Anatolian Crystalline Complex made of Late Cretaceous intrusions and Barrovian metamorphic rocks (e.g. Seymen, 1981; Göncüoğlu *et al.*, 1997; Aydın *et al.*, 1998; Whitney *et al.*, 2001) with inferred early Palaeozoic to Mesozoic protolith (Kocak & Leake, 1994; Göncüoğlu *et al.*, 1997). In the Late Cretaceous and early Cenozoic, arc magmatism above the north-dipping Neotethys subduction zone took place in the Pontides (Şengör & Yılmaz, 1981; Okay & Satır, 2006) and the Central Anatolian Crystalline Complex (Kadioğlu *et al.*, 2003; Ilbeyli *et al.*, 2004).

Western and Southern Anatolia consists of metamorphosed and non-metamorphosed Precambrian to Eocene rocks, known as the Anatolide–Tauride Block (Okay & Tüysüz, 1999). This domain is characterized by a Precambrian crystalline basement of Gondwana affinity (Pan-African orogeny, late Ordovician glaciation; Monod *et al.*, 2003), and Late Cretaceous to early Cenozoic H*P*–L*T* metamorphism that affected its northern passive margin (e.g. Şengör & Yılmaz, 1981; Pourteau *et al.*, 2010).

Anatolide–Tauride units

The term ‘Anatolides’ is used to designate the units affected by Alpine (i.e. Late Cretaceous to early Cenozoic) regional metamorphism, and the term ‘Taurides’ designates the non-metamorphosed thrust and folded external platform units (Fig. 1).

The Taurides, which consist of Precambrian to Eocene sedimentary rocks and Neotethyan ophiolites

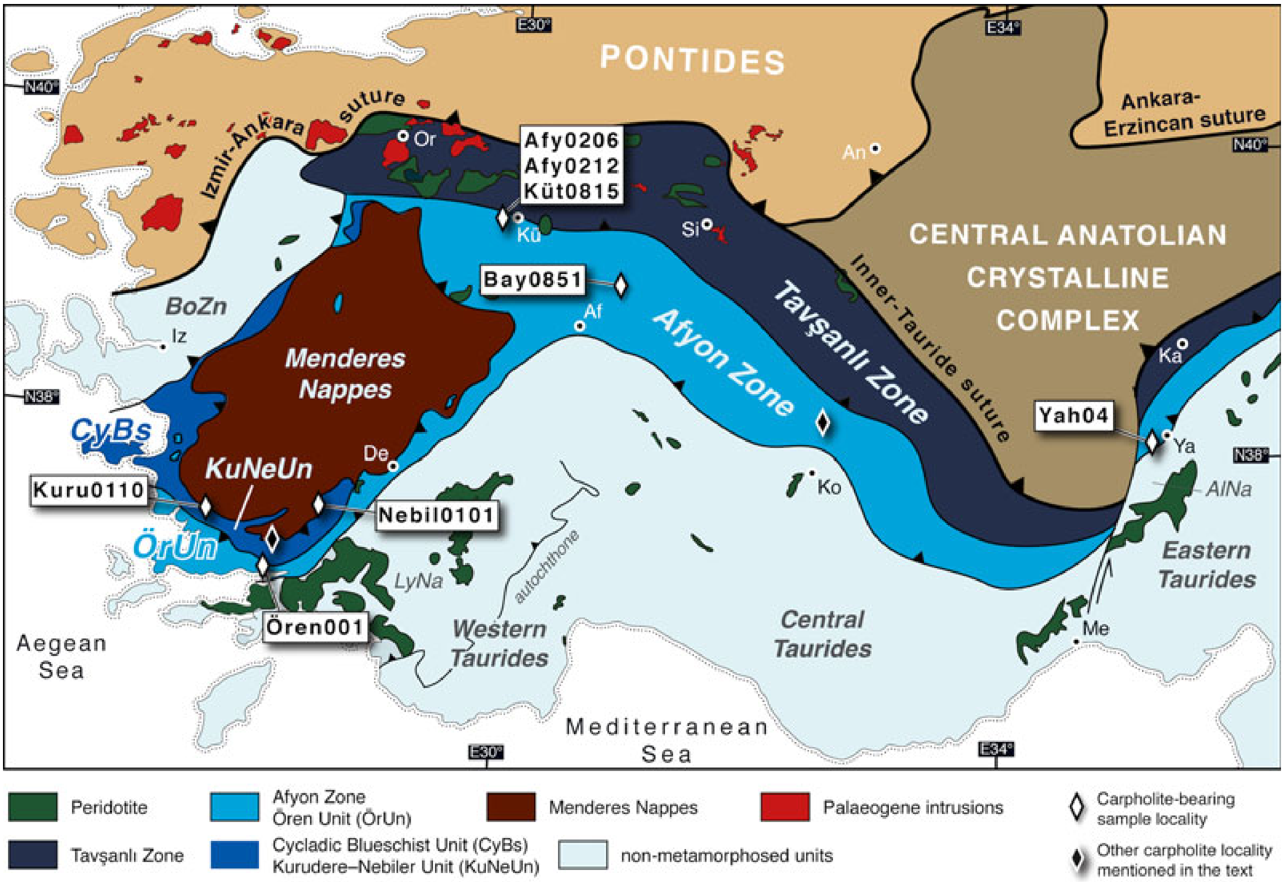

Figure 1. Tectonic units of Western and Central Anatolia (note the Ören Unit klippen atop the Cycladic Blueschist Unit and northern Menderes Nappes) and distribution of the carpholite-bearing samples used for ^{40}Ar–^{39}Ar geochronology in the present study. Other carpholite localities discussed in text are Bahçeyaka in the Kurudere–Nebiler Unit (Rimmelé *et al.*, 2003b), and Konya in the central Afyon Zone (Pourteau *et al.*, 2010). Unit abbreviations are: AlNa, Aladağ Nappes; BoZn, Bornova Zone; CyBs, Cycladic Blueschist Unit; HBHNa, Hoyran–Beyşehir–Hadim Nappes; LyNa, Lycian Nappes; ÖrUn, Ören Unit. Toponymic abbreviations are: Af, Afyonkarahisar; An, Ankara; De, Denizli; Iz, Izmir; Ka, Kayseri; Ko, Konya; Kü, Kütahya; Me, Mersin; Or, Orhaneli; Si, Sivrihisar; Ya, Yahyalı.

with 93–90 Ma–old metamorphic soles (Çelik *et al.*, 2006), were affected by multistage deformation between latest Cretaceous and late Miocene times, leading to the formation of regional-scale nappe systems (e.g. Lycian Nappes; Gutnic *et al.*, 1979; Collins & Robertson, 1998). The NW edge of the Menderes Nappes is thrust below the Bornova Zone, representing a non-metamorphosed, tectonized Maastrichtian–Danian ‘megaolistostrome’, which might have formed along a sinistral transform zone at the edge of the Anatolide–Tauride Block (Okay *et al.*, 1996).

Here the main characteristics and nomenclature of the western Anatolides, where it has been best described, are summarized and this tectono-stratigraphy is expanded eastwards. For further details, the reader is referred to Jolivet *et al.* (2013). The western Anatolides are composed of a metamorphosed Mesozoic sedimentary sequence, and its substratum represented by Precambrian high-grade metamorphic and intrusive rocks and Palaeozoic sedimentary and volcanic formations (e.g. Şengör & Yılmaz, 1981; Okay *et al.*, 1996). The general Mesozoic lithostratigraphy consists of a continuous succession of Triassic clastic sedimentary rocks (with volcanic intercalations) followed by Upper Triassic to Upper Cretaceous neritic carbonates followed by pelagic limestones, cherts, flysches, and olistostromes (e.g. Bozkurt & Oberhänsli, 2001). This sequence is interpreted as the continuous record of the development of a continental passive margin from rifting in the Early Triassic (e.g. Akal *et al.*, 2012) to oceanization in the middle Triassic, and later carbonate platform drowning in the Late Cretaceous, as it entered the trench of the north-dipping Neotethyan subduction zone (Okay *et al.*, 2001). Between the Late Cretaceous and the early Cenozoic, parts of the continental margin were metamorphosed in a subduction zone, as evidenced by the occurrence of widespread H*P*–L*T* minerals in Lower Triassic sedimentary and volcanic rocks (Okay *et al.*, 1996; Pourteau *et al.*, 2010).

Owing to contrasting lithostratigraphies and metamorphic grades, the Anatolides are subdivided into several tectonic units (Fig. 1).

The Tavşanlı Zone is a Late Cretaceous H*P*–L*T* metamorphic belt (Okay, 1984), derived from the most distal parts of the north-facing Anatolide-Tauride platform (Candan *et al*., 2005). In its western part, the Tavşanlı Zone is characterized by well-preserved lawsonite-glaucophane-bearing metasedimentary and metavolcanic rocks (including local lawsonite eclogite), for which peak *P*–*T* conditions were estimated to be 2.0–2.6 GPa and 430–550 °C (Okay & Kelley, 1994; Okay, 2002; Davis & Whitney, 2006, 2008; Çetinkaplan *et al*., 2008). Sporadic occurrence of blueschist blocks in mélange localities near Konya, in the Bolkar Mountains and near Kayseri (van der Kaaden, 1966; Droop *et al*., 2005) outlines the eastward continuation of the Tavşanlı Zone into Central Anatolia (Okay, 1984; Pourteau *et al*., 2010). Lawsonite blueschists from near Konya experienced 0.9–1.1 GPa and 375–450 °C (Droop *et al*., 2005). The good preservation of lawsonite throughout the unit indicates cooling during decompression. Isotopic dates obtained on blueschists from the Tavşanlı Zone bracket peak- to early retrograde stages between 88 and 78 Ma (^{40}Ar–^{39}Ar and ^{87}Rb–^{86}Sr on phengite; Table 1 and references therein), and subsequent exhumation during the latest Cretaceous and the Palaeocene (*c*. 60 Ma; ^{40}Ar–^{39}Ar on fine-grained phengite; Sherlock *et al*., 1999). East of Sivrihisar (Fig. 1), blueschist facies minerals were replaced by greenschist- to amphibolite facies Barrovian-type assemblages (e.g. chloritoid ± staurolite ± sillimanite; Whitney, 2002; Whitney *et al*., 2011) supposedly formed *c*. 60 Ma (^{40}Ar–^{39}Ar on muscovite; Seaton *et al*., 2009). Near Orhaneli and Sivrihisar, the Tavşanlı Zone is overlain by an ophiolitic complex, composed of peridotites and an accretionary complex (e.g. Okay, 1984). The tectonic contact between the H*P*–L*T* rocks and the ophiolites is sealed by early Eocene calc-alkaline intrusions derived from mantle wedge melts (Harris *et al*., 1994; Delaloye & Bingol, 2000).

The Afyon Zone, which occurs south of and structurally below the Tavşanlı Zone (Fig. 1), is a low-grade H*P* metamorphic belt (Pourteau *et al*., 2010), representing a Mesozoic continental passive margin, including a polymetamorphic Precambrian substratum (Candan *et al*., 2005). Fe-Mg-carpholite, glaucophane, and calcite pseudomorphs after aragonite documented throughout the Afyon Zone are evidence for blueschist facies metamorphism (Candan *et al*., 2005; Pourteau *et al*., 2010). Based on carpholite–chloritoid assemblages in metasedimentary rocks, metamorphic conditions experienced by the Afyon Zone were estimated to be 0.8–1.1 GPa and 250–350 °C (Candan *et al*., 2005; Pourteau, 2011). No isotopic date information is available yet for the metamorphic evolution of the Afyon Zone, but stratigraphic relations leave a possible interval between the Campanian (*c*. 83–70 Ma) olistostrom at the uppermost stratigraphic levels of the Afyon Zone (Özer & Tansel Öngen, 2012), and the late Palaeocene (*c*. 58–55 Ma) non-metamorphic sedimentary cover (Dirik *et al*., 1999; Candan *et al*., 2005).

Table 1. Summary of the published isotopic dates for H*P*–L*T* metamorphism in the Anatolides.

Unit/locality	Rock type	Dating method	Isotopic date	Error	Reference
*Tavşanlı Zone**					
Orhaneli	Lws-bearing metabasite	Ph Rb–Sr	79.7	1.6	Sherlock *et al.* (1999)
Orhaneli	Metachert	Ph Rb–Sr	78.5	1.6	Sherlock *et al.* (1999)
Sivrihisar	Lws-bearing metabasite	Ph Rb–Sr	82.8	1.7	Sherlock *et al.* (1999)
Sivrihisar	Metachert	Ph Rb–Sr	80.1	1.6	Sherlock *et al.* (1999)
Sivrihisar	Cld-bearing schist	Ph Ar–Ar	87.9	0.6	Seaton *et al.* (2009)
Afyon Zone					
Kütahya	Car–qz vein	Ph Ar–Ar	62.8	1.5	this study
Kütahya	Car–qz vein	Ph Ar–Ar	65.9	2.8	this study
Kütahya	Car–qz vein	Ph Ar–Ar	61.5	8.0	this study
Afyon	Car-bearing phyllite	Ph Ar–Ar	74.6	1.1	this study
Afyon	Car-bearing phyllite	Ph Ar–Ar	83.4	0.7	this study
Yahyalı	Car–qz vein	Ph Ar–Ar	65.7	0.2	this study
Yahyalı	Car–qz vein	Ph Ar–Ar	64.8	0.4	this study
Yahyalı	Car–qz vein	Ph Ar–Ar	66.7	0.4	this study
Ören Unit					
Milas	Red-green phyllite	Ph Ar–Ar	70-90		Ring & Layer (2003)
Ören	Car–qz vein	Ph Ar–Ar	62.6	0.4	this study
Ören	Car–qz vein	Ph Ar–Ar	59.4	0.7	this study
Ören	Car–qz vein	Ph Ar–Ar	60.3	0.3	this study
Kurudere–Nebiler Unit					
Kurudere	Car–ky-bearing qz vein	Ph Ar–Ar	45.9	2.0	this study
Nebiler	Ky-bearing microconglomerate	Ph Ar–Ar	26.5	0.8	this study
Cycladic Blueschist Unit (Anatolian part)					
Dilek	Ep-blueschist	Ph Ar–Ar	40.1	0.4	Oberhänsli *et al.* (1998) Ring *et al.* (2007)

*Other phengite Ar–Ar dates by Okay *et al.* (1998), Sherlock *et al.* (1999) and Sherlock & Kelley (2002) are not included due to common excess argon.

The Menderes Massif, which occurs as a regional tectonic window below the other metamorphic units, exhibits a complicated internal structure (e.g. Şengör *et al*., 1984; Gessner *et al*., 2001c; Okay, 2001; Ring *et al*., 2001). Yet, a general lithostratigraphy was restored. It consists of a polymetamorphic (Pan-African and Alpine metamorphisms; Candan *et al*., 2011) gneiss core overlain by monometamorphic Palaeozoic schist and Mesozoic marble covers, and a Palaeogene olistostrome (Schuiling, 1962; Dürr, 1975; Özer *et al*., 2001). The Menderes Massif is generally characterized by Barrovian-type metamorphism (Bozkurt & Oberhänsli, 2001; Gessner *et al*., 2001a; van Hinsbergen, 2010) with *P*–*T* conditions (estimated in monometamorphic Palaeozoic schists from the southern Menderes Massif) of 0.4–0.5 GPa and 330–530 °C (monometamorphic Palaeozoic schists from the southern Menderes Massif; Whitney & Bozkurt, 2002; Régnier *et al.*, 2003). In the same region, Fe-Mg-carpholite relicts were described at the base of the Mesozoic carbonate sequence, as evidence for H*P*–L*T* metamorphism in this part of the massif (Rimmelé *et al.*, 2003b; Whitney *et al.*, 2008). The preservation of carpholite (i.e. the occurrence of relicts *vs.* pseudomorphs) correlates with that of diaspore in metabauxite horizon in platform-type marbles (Rimmelé *et al.*, 2003b), as also mentioned in the Cycladic Blueschist Unit (Candan *et al.*, 1997). *P*-*T* estimates are 1.2–1.4 GPa/470–550 °C in Kurudere (location of sample Kuru0110; Fig. 1), 0.6–0.8 GPa/400–450 °C in Bahçekaya, and 0.9–1.1 GPa/380–480 °C in Nebiler (location of sample Nebil0101; Fig. 1) (Rimmelé *et al.*, 2003b, 2005; Whitney *et al.*, 2008). This H*P*–L*T* metamorphic event probably affected the entire Mesozoic marble sequence, described as stratigraphically continuous (Dürr, 1975; Özer *et al.*, 2001), but not the Palaeozoic schist cover, which, in parts is only affected by low-grade conditions (chlorite zone; Schuiling, 1962), lacks H*P* minerals. Therefore, in this region, only the marble cover (including basal conglomerates containing carpholite relicts) is considered to have experienced H*P*–L*T* metamorphism. Hence, the Menderes Massif *sensu lato* is sub-divided into the low- to middle-*P* Menderes Nappes (Gessner *et al.*, 2001a), and the newly termed H*P*–L*T* Kurudere–Nebiler Unit (Fig. 1). The timing of this H*P*–L*T* metamorphism was not yet estimated by means of isotopic dating methods, but it is predated by the middle Palaeocene depositional age of the olistostrome topping the Cretaceous marble (Özer *et al.*, 2001), and probably post-dated by the Barrovian metamorphism the Menderes Massif underwent. Available isotopic dates for the metamorphic evolution of the Menderes Massif *sensu lato* (^{40}Ar–^{39}Ar and ^{87}Rb–^{86}Sr on white mica and biotite) are scattered between *c*. 62 and 27 Ma (Satır & Friedrichsen, 1986; Bozkurt & Satır, 2000; Lips *et al.*, 2001). Therefore, the H*P*–L*T* metamorphic history of the Kurudere–Nebiler Unit likely occurred sometime between the late Palaeocene and the Eocene. It is noteworthy that Ring *et al.* (1999) regarded most of the Mesozoic cover of the entire Menderes Massif *sensu lato* as the continuation of the Cycladic Blueschist Unit, even parts free of H*P* relicts.

The Ören Unit (Pourteau *et al.*, 2010), formerly referred to as the metamorphosed part of the Lycian Nappes (Oberhänsli *et al.*, 2001; Rimmelé *et al.*, 2003a), lies structurally over the Kurudere–Nebiler Unit, the Menderes Nappes, and the Cycladic Blueschist Unit (Fig. 1). Kinematic indicators (Rimmelé *et al.*, 2003a, 2006) indicate that, during the late stage of its exhumation, the Ören Unit was transported over these units towards the ESE (after restoration from the Neogene extensional deformation; Pourteau *et al.*, 2010; van Hinsbergen, 2010). Fe-Mg-carpholite in the lower metasedimentary rocks and calcite pseudomorphs after aragonite in marbles are widespread evidence for blueschist facies metamorphism (Oberhänsli *et al.*, 2001; Rimmelé *et al.*, 2003a, 2006). Peak *P*–*T* conditions were estimated to be ~1.2 GPa and 400 °C (Rimmelé *et al.*, 2005). Rocks near the base of the Ören Unit (including the klippen) experienced isothermal decompression at ~400–450 °C, whereas rocks at higher tectonostratigraphic positions experienced cooling during decompression (Rimmelé *et al.*, 2005). This shows that the thermal evolution of H*P*–L*T* rocks during their exhumation can significantly vary within a single tectonic unit. ^{40}Ar–^{39}Ar dates between 90 and 70 Ma were obtained on phengite from metasedimentary rocks as the only isotopic estimate for the metamorphism of the Ören Unit (Ring & Layer, 2003). Stratigraphic relations bracket the H*P*–L*T* metamorphic event in a latest Cretaceous to Eocene interval (Rimmelé *et al.*, 2003a). Owing to its structural position, metamorphic evolution and lithostratigraphy, the Ören Unit might represent the western continuation of the Afyon Zone.

In Western Anatolia, the Cycladic Blueschist Unit, which is otherwise widely exposed in Aegea, consists of two H*P* metamorphic units (a lower platform sequence and an upper metamorphic mélange) that lie tectonically over the western Menderes Nappes (Candan *et al.*, 1997; Oberhänsli *et al.*, 1998; Ring *et al.*, 1999; Okay, 2001). Peak *P*–*T* estimates are 1.1–1.5 GPa and 440–550 °C (Çetinkaplan, 2002; Ring *et al.*, 2007). Available phengite ^{40}Ar–^{39}Ar dates indicate exhumation between *c*. 40 and 32 Ma, along an isothermal decompression path through the greenschist facies (Oberhänsli *et al.*, 1998; Ring *et al.*, 2007). This is consistent with H*P* metamorphic timing in the Cycladic Blueschist Unit in Aegea (e.g. Jolivet & Brun, 2008; Ring *et al.*, 2010), where the metamorphic peak was dated to *c*. 52 Ma (^{176}Lu-^{176}Hf on eclogitic garnet; Lagos *et al.*, 2007).

Several tectonic units of the Anatolide–Tauride Block are topped by widespread ophiolites (Fig. 1) that were generated above a subduction zone (e.g. Önen & Hall, 1993; Parlak *et al.*, 1996). Greenschist- to amphibolite facies sub-ophiolitic metamorphic soles formed during subduction initiation were dated to 93–90 Ma (e.g. Robertson, 2002; Çelik *et al.*, 2006).

P–*T* ESTIMATION AND ^{40}Ar–^{39}Ar GEOCHRONOLOGY

Fe-Mg-carpholite in metasedimentary rocks is the main, or locally the only evidence of ‘Alpine’ H*P*–L*T* metamorphism in the Afyon Zone, the Ören Unit and the Kurudere–Nebiler Unit. Phengite, typically accompanied by chlorite, commonly occurs in carpholite-bearing rocks, offering the chance to determine the timing of metamorphism by using ^{40}Ar–^{39}Ar geochronology. Several studies previously showed that this approach yields reliable metamorphic dates (e.g. Jolivet *et al.*, 1996; Agard *et al.*, 2002; Wiederkehr *et al.*, 2009; Oberhänsli *et al.*, 2012). In these rocks, white mica may have formed before, during and after carpholite growth, so several generations can coexist in a single sample and thus provide various isotopic dates (e.g. Agard *et al.*, 2002; Wiederkehr *et al.*, 2009). To evaluate the possibility of such situations, *P–T* conditions prevailing during the growth of the dated white mica can be estimated by chlorite–phengite thermobarometry (multi-equilibrium approach; Vidal & Parra, 2000) (see below). Therefore, when possible, $^{40}Ar–^{39}Ar$ dating was combined with *P–T* estimation in individual samples to decipher the significance of isotopic dating results.

Sample selection

Selection criteria

For $^{40}Ar–^{39}Ar$ geochronology, selected samples contain white mica that (i) is rich in potassium and poor in sodium (phengitic *v.* paragonitic mica); (b) is obviously of metamorphic origin; (c) occurs as medium-sized to coarse crystals (> 125 μm); (d) is not intergrown with chlorite or pyrophyllite; and (e) was not affected by late fluid circulation (i.e. no fractures, no late calcite crystallization). Bearing in mind that carpholite-bearing quartz veins originate from the crystallization of a fluid phase under H*P*–L*T* conditions, white mica in such a rock type is exclusively of metamorphic origin. Therefore, to avoid the risk of the radiogenic Ar inheritance of detrital mica recrystallized during metamorphism, quartz vein samples were preferentially selected.

Selected samples

Because both fine grain size and common intergrowth of white mica with chlorite critically restrict sample selection, a total of nine samples were selected, six from the Afyon Zone, one from the Ören Unit, and two from the Kurudere–Nebiler Unit. Carpholite-bearing rocks in the Afyon Zone are mostly quartz segregations (or 'veins'), and also quartz–mica schists and pyrophyllitite (Candan *et al.*, 2005; Pourteau, 2011). Veins typically consist of the assemblage quartz + carpholite ± pyrophyllite ± chlorite ± chloritoid. Phengite and paragonite are more rarely observed. Samples Afy0206, Afy0212 and Küt0815 were collected from the area near Kütahya (Fig. 1; Table S2). In sample Afy0206, phengite and chlorite occur as needle-shaped associations that are up to 2 cm in length, and carpholite is observed only as tiny fibres in quartz (Fig. 2a). This suggests that large needles of carpholite were consistently pseudomorphed to white mica and chlorite through the continuous, decompression reaction carpholite + phengite = chlorite + muscovite + quartz + water (R1; e.g. Bousquet *et al.*, 2002), whereas tiny needles, included in quartz, were preserved. Phengite and chlorite are typically intergrown, but pseudomorphs are locally only composed of phengite. *In situ* laser ablation therefore was the most suitable method to extract Ar from selected chlorite-free domains (Fig. 2a). The sample Afy0212 was described by Pourteau (2011) for remarkable carpholite–chloritoid textures. Pyrophyllite, which occurs as large crystals wrapping carpholite and chloritoid, contains discrete layers of celadonite-poor (X_{Cel} = 0.04), muscovite-rich phengite. In sample Küt0815, carpholite is rather well preserved, but displays evidence for local breakdown into chlorite and pyrophyllite that here again contains thin celadonite-poor (X_{Cel} = 0.02) phengite interlayers. To extract enough Ar for isotope analysis from these pyrophyllite–phengite composite grains, stepwise heating was applied on separated grains from these two samples.

In the region of Afyon city, carpholite-bearing metapelites and metaconglomerates contain abundant, fine-grained phengite, intergrown with pyrophyllite, quartz and iron oxides, but notably no chlorite (Candan *et al.*, 2005; Pourteau, 2011). Sample Bay0851 (Fig. 1; Table S2) is a carpholite-bearing silvery phyllite (Fig. 2b). The notable absence of chlorite in this sample, on the one hand, prevents its use for accurate *P–T* estimation, but, on the other hand, indicates that the peak mineral assemblage (represented by carpholite and chloritoid) was well preserved. Most matrix phengite is poor in celadonite (X_{Cel} = 0.01–0.08). By contrast, phengite in contact with carpholite fan-shaped aggregates yields X_{Cel} values up to 0.32, and is thus among the highest-*P* phengite found in the Afyon Zone. This suggests that Ar isotope analysis in this sample might provide near-peak metamorphic dates. With the aim of analysing higher-*P* and lower-*P* phengite distinctively, sample Bay0851 was prepared for *in situ* laser ablation.

In the Konya region (Fig. 1), some carpholite-quartz veins also contain white mica, but this contains a significant paragonite component, preventing any accurate *P–T* estimation and, a priori, hampering $^{40}Ar–^{39}Ar$ geochronological investigations. Ar isotope analysis was tentatively performed on a sample from the region of Konya (Kon0316; Fig. 1; Table S2), but laser ablation experiments did not release any significant gas amount for Ar isotope analysis.

In the easternmost regions of Yahyalı and Kayseri (Fig. 1; Table S2), carpholite, which is again observed only as isolated fibres in quartz, was substantially pseudomorphed by phengite and chlorite through the reaction R1. Chloritoid also occurs locally among phengite–chlorite associations, probably as a result from the progressive prograde reaction carpholite = chloritoid + quartz + water (R2; Chopin & Schreyer, 1983). In the sample Yah04 that was selected, phengite and chlorite are mostly intergrown, but also occur as isolated crystals, allowing easy mineral separation.

In the Ören Unit, carpholite-bearing quartz veins commonly contain peak to retrograde phengite and

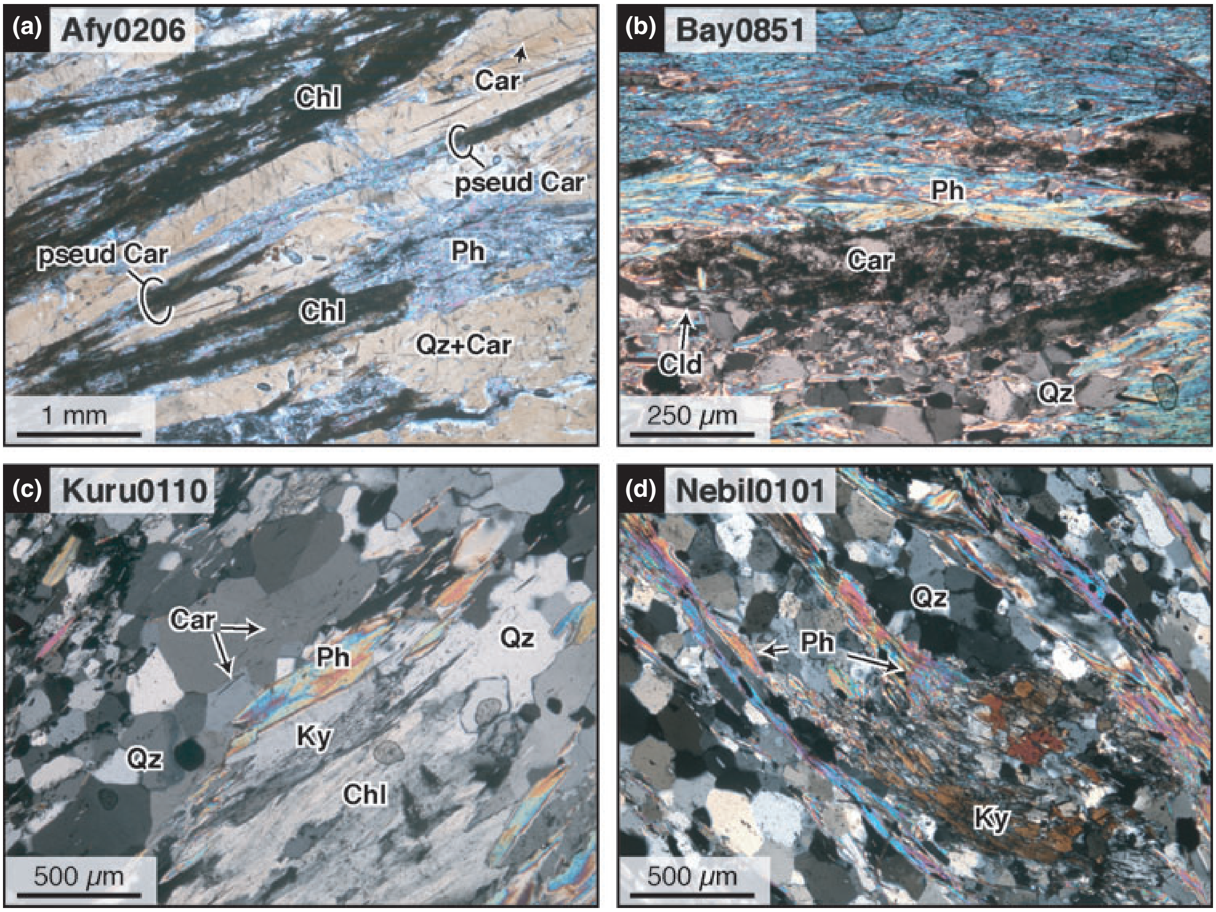

Figure 2. Optical microphotographs (cross polars) of the samples investigated by in situ UV laser ablation. a) Retrograde phengite and chlorite occurs as needle-like pseudomorphs after carpholite, preserved only as fibres included in quartz, in Afy0206 (western Afyon Zone). b) Pre-foliation, near-peak phengite is observed among quartz and carpholite, whereas syn-foliation, retrograde phengite constitutes most of the schistose matrix in phyllite Bay0851 (central Afyon Zone). c) Textural equilibrated retrograde phengite, kyanite and chlorite formed due to the breakdown of carpholite (fibres in quartz) in Kuru0110 (western Kurudere–Nebiler Unit). d) Late retrograde white mica grew during the development of post-kyanite foliation in Nebil0101 (eastern Kurudere–Nebiler Unit). Mineral abbreviations are after Whitney & Evans (2010).

chlorite (Oberhänsli *et al.*, 2001; Rimmelé *et al.*, 2003a, 2005). The selected sample Ören001 (Fig. 1; Table S2) stemmed from a quartz vein encompassing well-preserved carpholite needles partly replaced by phengite and chlorite (Rimmelé *et al.*, 2003a). In this sample, carpholite–chlorite–phengite–quartz–water multi-equilibrium calculations yielded *P–T* conditions of 0.8–1.1 GPa and 320–380 °C (Rimmelé *et al.*, 2005).

From the Kurudere–Nebiler Unit, two samples previously studied by Rimmelé *et al.* (2003b, 2005) were selected: Kuru0110, located at the diaspore–corundum isograd, and Nebil0101, located within the corundum zone. Sample Kuru0110 is a quartz vein containing the main assemblage kyanite + chlorite + phengite + pyrophyllite + carpholite. Kyanite, chlorite and phengite, observed in equilibrium textures, whereas carpholite occurs only as fibres included in quartz (Fig. 2c). Phengite therefore grew coevally with the products of the reaction carpholite = chlorite + kyanite + quartz + water (e.g. Azañon & Goffé, 1997; Rimmelé *et al.*, 2003b). The eastern sample Nebil0101 is a metamorphosed quartz micro-conglomerate containing kyanite + chloritoid + phengite as the main assemblage. Chlorite was reported to be abundant in this sample (Rimmelé *et al.*, 2003b), but was not seen in the selected sample fragment. Furthermore, no carpholite relict was observed in this sample, whereas kyanite–chlorite pseudomorphs after carpholite were described from the same locality. In the selected rock fragment, scarce phengite layers among the recrystallized quartz matrix define a weak foliation that wraps crystals of kyanite (Fig. 2d) and chloritoid, and therefore probably post-date their formation.

P–T estimation – analytical methods

Metamorphic *P–T* conditions for samples Afy0206 and Yah04 (western and eastern Afyon Zone, respectively) were estimated using chlorite–quartz–water thermometry (Vidal *et al*., 2005, 2006), phengite–quartz–water thermobarometry (Dubacq *et al*., 2010), and the chlorite–phengite–quartz–water multi-equilibrium approach first proposed by Vidal & Parra (2000) and subsequently applied in many different geological contexts (e.g. Trotet *et al*., 2001, 2006; Parra *et al*., 2002; Arkai *et al*., 2003; Vidal *et al*., 2006; Ganne *et al*., 2012; Grosch *et al*., 2012; Lanari *et al*., 2012a,b). When possible (sample Yah04), *P–T* conditions were also estimated from chlorite–chloritoid–quartz–water assemblages.

Mineral composition analysis

Element mapping (for Si, Al, Fe, Mg, K and Na) combined with spot analysis was performed using an electron microprobe JEOL JXA8200 (Potsdam University), following the procedure described by De Andrade *et al*. (2006). Areas selected for mapping contain the coarsest grains possible and display sharp grain boundaries (i.e. limited intergrowths). Operating conditions for maps were 15 keV accelerating voltage, 5 μm beam size, 100 nA beam current, for counting times of 300 ms on peak. Spot analyses were acquired with 15 keV accelerating voltage, 5 μm beam size, 10 nA beam current, for counting times of 20 s on peak and 10 s on background. Standards of pyrope for Si, rutile for Ti, pyrope for Al, hypersthene for Fe, fayalite for Mn (to analyse accurately very low amount of Mn), diopside for Mg, diopside for Ca, anorthite for Na, and microcline for K were used.

A distinct chemical phase (chlorite, phengite, quartz, Ti oxide; Fig. 3–b–b') was attributed to each pixel of the element maps using *XMapTools* software (Lanari *et al*., 2012a,b, 2013; http://www.xmaptools.com). Then, profiles of individual spot quantitative analyses traced across phengite–chlorite aggregates were used as standards to obtain a quantitative analysis (in oxide weight percent) from each pixel of the qualitative element maps. Therefore, in each investigated area, a large number of spot analyses were acquired for each phase to ensure the precision of this quantification. Structural formula and atom site repartition for each pixel of chlorite and phengite were calculated using the functions *Chl-StructForm* and *Phg-StructForm* in *XMapTools*, following the solid solution models of Vidal & Parra (2000), Vidal *et al*. (2006) and Dubacq *et al*. (2010). Chlorite and phengite pixels were then distributed into various composition groups using the K-means clustering method (Saporta, 1990) for each of which an average composition was calculated.

In addition, the presence of very fine-grained chloritoid in Yah04, albeit not allowing element mapping, allowed calculation of *P–T* conditions prevailing for local chlorite–chloritoid–quartz–water equilibrium (see detail below). The composition of chloritoid and chlorite in equilibrium textures was determined through individual spot analysis.

Chlorite–quartz–water thermometry

The evolution of chlorite composition with the temperature (e.g. Vidal *et al*., 2001) in equilibrium with quartz and water can be modelled using the two independent equilibria (Vidal *et al*., 2005, 2006):

$$5\text{Mg-amesite} + 4\text{daphnite} \leftrightarrow 4\text{clinochlore} + 5\text{Fe-amesite} \quad (1)$$

$$4\text{daphnite}+6\text{sudoite}\leftrightarrow 3\text{Mg-amesite}+5\text{Fe-amesite}+14\text{quartz}+8H_2O \quad (2)$$

where Mg-amesite, Fe-amesite, daphnite, sudoite and clinochlore are chlorite end-members. The activities of these end-members were calculated using the thermodynamic data and the activity model used in Vidal *et al*. (2006). For any given pressure, the temperature of crystallization and the ferric iron content (X_{Fe3+}) of chlorite were simultaneously estimated using criterion based on the convergence of the equilibria (1) and (2). Following the strategy previously detailed in Lanari *et al*. (2012a), T and X_{Fe3+} of chlorite were estimated at a fixed pressure of 4 kbar and a water activity equal to 1. Convergence was assumed when the temperature difference between the two equilibria was < 30 °C. Each chlorite group was considered individually to calculate a temperature using the chlorite–quartz–water equilibrium (at a given pressure) following the method of Vidal *et al*., (2005); Vidal *et al*. (2006). Results are displayed as maps of chlorite temperatures (Fig. 3b-b').

Phengite–quartz–water barometry

The equilibrium conditions of the assemblage phengite + quartz + water can be modelled using the following three equilibria (among which two are independent):

$$3\text{celadonite} + 2\text{pyrophyllite} \leftrightarrow 2\text{muscovite} + \text{biotite} + 11\text{quartz} + 2H_2O \quad (3)$$

$$3\text{celadonite} + 2\text{pyrophyllite} \cdot 1H_2O \leftrightarrow 2\text{muscovite} + \text{biotite} + 11\text{quartz} + 3H_2O \quad (4)$$

$$\text{pyrophyllite} \cdot 1H_2O \leftrightarrow \text{pyrophyllite} + H_2O \quad (5)$$

where celadonite, pyrophyllite, pyrophyllite·$1H_2O$, muscovite and biotite are the end-members of phengite. The activities of these end-members were calculated using the thermodynamic data and activity model used in Dubacq *et al*. (2010). Equilibrium convergence at various *P–T* conditions was achieved by changing the amount of interlayer water (i.e. the proportion of pyrophyllite·$1H_2O$). For the average composition of each phengite group (except for muscovite–paragonite textures), the method of Du-

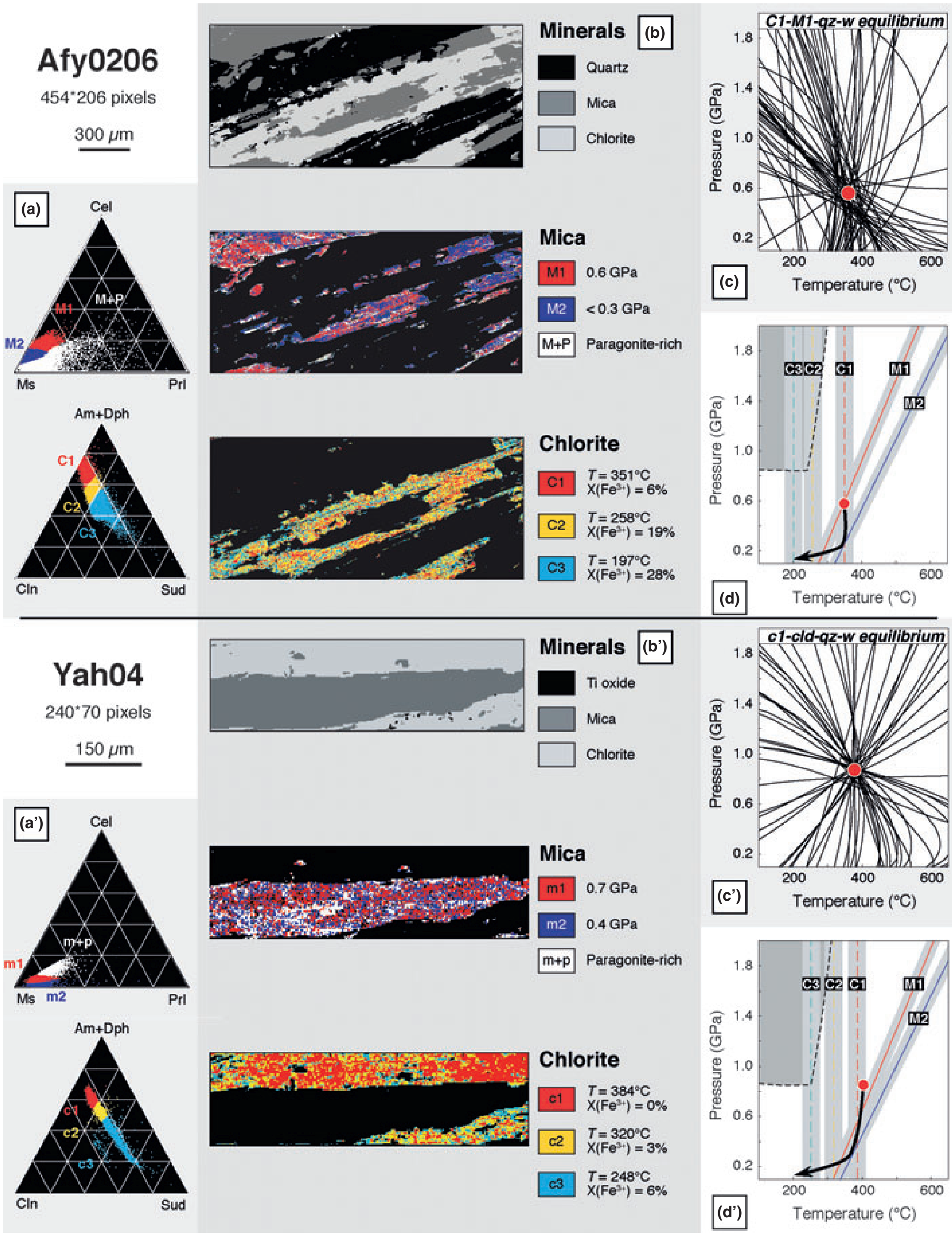

Figure 3. Results of multi-equilibrium thermobarometry for the samples Afy0206 and Yah04. a) and a') Ternary diagrams for white mica and chlorite compositions. Each point represents the composition of one pixel. Colours indicate the statistical composition groups mentioned in the text. Mineral abbreviations are after Whitney & Evans (2010). b) and b') Map views of phase distribution, and mica pressure– and chlorite temperature groups in the investigated areas. "XF" stands for Fe^{3+}/Fe_{total} in chlorite. c) and c') chlorite–phengite–quartz-water (Afy0206) and chlorite–chloritoid–quartz–water (Yah04) multi-equilibrium calculations using average group compositions. d) and d') Result summary. Grey fields represent the stability fields of carpholite with Mg/(Mg+Fe) = 0.30 (d) and 0.35 (d'), calculated with TheriakDomino (De Capitani & Petrakakis, 2010) following Pourteau (2011). See text for details.

bacq *et al*. (2010) was used to plot a P–T line corresponding to the phengite–quartz–water equilibrium, with variable hydration states (see the method description above). Phengite equilibrium pressure and hydration state were then estimated at the temperatures of the chlorite–quartz–water equilibria (Lanari *et al*., 2012a). Results are displayed as maps of phengite pressures in Fig. 3–b–b'.

Chlorite–phengite–quartz–water thermobarometry

Once chlorite–quartz–water thermometry and phengite–quartz–water barometry were applied, thermodynamic equilibrium between each chlorite group and each phengite group was tested through a full chlorite–phengite multi-equilibrium approach involving X_{Fe3+} in both minerals. P–T equilibrium conditions of chlorite–phengite–quartz–water assemblages were calculated from the convergence of 64 equilibria obtained from the chlorite and phengite end-members mentioned above (details in Vidal *et al*., 2006). Only equilibria showing a good convergence were selected.

Chlorite–chloritoid–quartz–water thermobarometry

P–T equilibrium conditions for chlorite–chloritoid–quartz–water assemblage were calculated from the convergence of 39 (three independent) equilibria obtained from the chlorite end-members mentioned above with Mg-chloritoid and Fe-chloritoid (thermodynamic data from JUN92.bs database, updated from Berman (1988)). Only equilibria showing a good convergence were selected. This thermobarometer was applied to Yah04 using individual spot analyses of chlorite and chloritoid observed in equilibrium textures.

P–T **estimation – results**

Mineral analyses in Afy206 and Yah04

Whereas under the optical microscope chlorite and white mica seem to have formed during a single event (carpholite breakdown reaction R1), several composition groups, and thence P- and T groups, can be distinguished for each phase. In each sample, the statistical analysis gave chlorite pixel distributions of three compositional groups: C1 to C3 (upper case) in Afy0206, and c1 to c3 (lower case) in Yah04. On the other hand, three compositional groups were also distinguished for mica pixels: M1, M2, M + P in Afy0206, and m1, m2, m + p in Yah04, where M + P and m + p stand for muscovite–paragonite mixtures. Average compositions for each of these groups, except the muscovite–paragonite mixtures, are shown in Table 2. In both samples, chlorite compositional groups display an increase in the sudoite-content from C1 to C3 and from c1 to c3, but no significant change in the proportion of the other end-members (Fig. 3–a–a' and Table 2). Sudoite-richest compositions (C3 and c3) tend to occur in external parts of chlorite aggregates (Fig. 3–b–b'). Because, at fixed bulk rock composition, the abundance of the sudoite end-member (vacancy on the octahedral site [M1]) decreases with increasing temperature (Cathelineau & Nieva, 1985; Hillier & Velde, 1991; Vidal *et al*., 2001), this zoning trend indicates that chlorite grew during cooling. This supports the statement that chlorite is the product of carpholite retrogression. On the other hand, celadonite-content in phengite, thus its Si content, increases with pressure (Bousquet *et al*., 1998; Agard *et al*., 2001). Therefore, owing to higher celadonite-contents, phengite M1 formed at higher pressure than M2 (X_{Cel} = 0.16 *v.* 0.04), and m1 grew at slightly higher pressure than m2 (X_{Cel} = 0.04 *v.* 0.02) (Fig. 3–a–a'; Table 2). Since phengite formed through the decompression reaction R1, higher-P M1 and m1 phengites probably formed earlier than M2 and m2, respectively. Carpholite in Afy0206 and Yah04 gives X_{Mg} values of 0.5 and 0.3–0.4, respectively. Chloritoid analysis in Yah04 reveals that, from grain to grain, X_{Mg} varies between 0.12 and 0.22 (e.g. Table 3).

Thermobarometric results

In Afy0206, chlorite–quartz–water thermometry using the C1, C2, and C3 chlorite average compositions provides temperatures of ~351, 258 and 197 ± 50 °C and X_{Fe3+} of 6, 19 and 28% respectively (Table 2). The two phengite P–T equilibrium lines obtained from phengite–quartz–water barometry intersect only with the C1 chlorite line (T = 350 °C). Intersection points indicate for M1 and M2 mica pressures of 0.6 and < 0.3 GPa respectively. In addition, multi-equilibrium calculations using group average compositions reveal thermodynamic equilibrium between C1 chlorite and M1 mica, and yield estimates of ~0.6 GPa and ~350 °C (Fig. 3c). These P–T conditions are consistent with those determined individually using chlorite–quartz–water and phengite–quartz–water equilibria.

In Yah04, chlorite–quartz–water thermometry yields temperatures of 384, 320 and 248 ± 50 °C (at 1.0 GPa) and X_{Fe3+} of 6, 19, and 28% for the c1, c2 and c3 chlorite groups respectively (Table 2). Here again, the two phengite P–T equilibrium lines obtained for m1 and m2 intersect the highest-T chlorite (c1, at 380 °C; Fig. 3d') at 0.7 and < 0.4 GPa, respectively. Unfortunately, no equilibrium was found between the c1 chlorite and the m1 mica, but an equilibrium was identified between the c1 chlorite and average chloritoid composition (X_{Mg} = 0.14) at ~0.6 GPa and ~350 °C (Fig. 3c'). In addition, P–T conditions calculated for individual chlorite–chloritoid pairs of spot analyses range between 0.82 and 1.13 GPa, and between 383 and 425 °C (Table 3). Therefore, chloritoid growth, out of the carpholite stability field (Fig. 3d'), probably represents the HP thermal climax experienced by this sample.

Table 2. Calculated average compositions of chlorite and mica groups in samples Afy0206 and Yah04 (see details in the text).

Chlorite	Afy0206			Yah04		
	C1	C2	C3	C1	C2	C3
SiO_2	25.25	26.39	27.51	25.75	26.57	27.93
Al_2O_3	21.88	22.83	22.71	25.68	26.24	27.14
FeO	27.59	26.33	25.06	22.45	21.52	20.06
MnO	0.06	0.06	0.06	0.05	0.05	0.05
MgO	11.55	11.60	11.22	14.59	14.07	13.23
CaO	0.09	0.09	0.09	0.02	0.02	0.02
Na_2O	0.04	0.04	0.04	0.06	0.13	0.25
K_2O	0.35	0.48	0.69	0.04	0.07	0.14
Atom site distribution (14 anhydrous oxygen basis including Fe^{3+})						
Si(T1 + T2)	2.67	2.74	2.82	2.62	2.68	2.77
Al(T2)	1.33	1.26	1.18	1.38	1.32	1.23
Al(M1)	0.33	0.26	0.18	0.38	0.32	0.23
Mg(M1)	0.23	0.21	0.20	0.25	0.24	0.22
Fe2 + (M1)	0.30	0.22	0.18	0.22	0.20	0.18
V(M1)	0.14	0.31	0.44	0.15	0.24	0.37
Mg(M2 + M3)	1.59	1.58	1.52	1.96	1.87	1.73
Fe^{2+}(M2 + M3)	2.00	1.63	1.37	1.69	1.58	1.39
Al(M2 + M3)	0.34	0.69	0.99	0.32	0.51	0.81
Al(M4)	0.85	0.57	0.40	1.00	0.96	0.90
Fe^{3+}(M4)	0.15	0.43	0.60	0.00	0.04	0.10
X(Fe^{3+}) (%)	6	19	28	0	3	6
Temperature (°C)*	351	258	197	384	320	248

	Afy0206		Yah04	
Mica	M1	M2	M1	M2
SiO_2	48.13	47.19	47.78	47.55
Al_2O_3	32.55	33.60	35.85	36.11
FeO	2.25	2.07	0.40	0.40
MnO	0.01	0.01	0.01	0.01
MgO	0.96	0.84	0.45	0.42
CaO	0.04	0.04	0.03	0.03
Na_2O	1.05	1.36	1.10	1.31
K_2O	9.21	8.86	8.86	8.39
Atom site distribution (11 anhydrous oxygen basis including Fe^{3+})				
Si(T1 + T2)	3.23	3.17	3.15	3.14
Al(T2)	0.77	0.83	0.85	0.86
V(M1)	0.98	0.97	1.00	0.99
Mg(M1)	0.01	0.01	0.00	0.01
Fe(M1)	0.01	0.02	0.00	0.00
Al(M2 + M3)	1.80	1.83	1.94	1.95
Mg(M2 + M3)	0.09	0.07	0.04	0.03
Fe(M2 + M3)	0.11	0.10	0.02	0.02
K(A)	0.79	0.76	0.75	0.71
Na(A)	0.13	0.17	0.14	0.17
V(A)	0.08	0.07	0.11	0.12
Prl	0.07	0.06	0.11	0.12
Tri	0.02	0.03	0.01	0.01
Prg	0.14	0.18	0.14	0.17
Ms	0.61	0.62	0.70	0.68
Cel	0.16	0.11	0.04	0.02

*Vidal *et al.* (2006), initial pressure = 0.5 GPa.

^{40}Ar–^{39}Ar geochronology

Phengite was extracted from samples Afy0212, Küt0815, Yah04, and Ören001 to perform Ar extraction by stepwise heating of separated grains with a CO_2 laser. Pure phengite grain bunches were obtained by scratching gently the freshly cut surface of the quartz vein samples followed by enrichment and purification using conventional techniques for mineral separation, including washing, sieving, adherence to paper, and handpicking under binoculars. To perform Ar extraction dating by *in situ* UV laser ablation, 1 mm thick, polished rock chips were prepared from the samples Afy0206, Bay0851, Kuru0110, and Nebil0101. Analytical procedure for ^{40}Ar–^{39}Ar analysis is described in Appendix S1. Ar release spectra obtained by stepwise heating of bulk grain samples were produced from bunches of three to seven grains of size ranging between 125 and 500 μm, which were heated by scanning laser beam with a diameter of 1600 μm for 45–90 s with 70 $\mu m\ s^{-1}$ scan speed. *In situ* UV laser ablation was carried out with a beam with a diameter of 50 μm and a 5 $\mu m\ s^{-1}$ scan speed. To release sufficient gas amounts in fine-grained phengite domains, the *in situ* ablation was performed following long paths (up to 1 500 μm) at the detriment of the textural resolution. For this reason, Ar isotope analysis may have yielded mixed dates for several coexisting generations of phengite (in Bay0851 in particular). Data have been corrected for blank, mass discrimination, decay of radiogenic ^{37}Ar and ^{39}Ar, and interference of Ar isotopes derived from K and Ca (Table S3).

Raw dating results

Details results of Ar isotope analyses are shown in Table S4. Representative Ar release diagrams are presented in Fig. 4. A significant plateau date is defined by a series of adjacent steps, which represent individually more than 5% and in all more than 50% of the total ^{39}Ar released during step heating and contiguously agree within 2-SD error limits (McDougall & Harrison, 1999). The Ar release spectra obtained fully satisfy these conditions. On the other hand, ^{40}Ar–^{39}Ar dates obtained by *in situ* laser ablation are displayed in 'pseudo-plateau' diagrams (Fig. 4b) in which dates are sorted in ascending order. This allows the representation of each spot analysis in terms of released gas amount.

Afyon Zone. *In situ* laser ablation of white mica in Afy0206 provided isotopic dates scattered from 47.1 ± 3.8 to 66.4 ± 6.1 and 80.6 ± 20.8 Ma, without apparent correlation between date, atmospheric Ar content and released gas amount. Five of the 10 steps, representing ~52% of the total ^{39}Ar release, give an average date of 62.8 ± 1.5 Ma (Fig. 4b). Stepwise heating of white mica separated from Küt0815 yielded a rather imprecise plateau for which a date of 65.9 ± 2.8 Ma was calculated (Fig. 4a). From Afy0212, consistent, albeit imprecise, dates were obtained for each of the seven steps from which four, representing 86% of the total ^{39}Ar release, indicate a plateau date of 61.5 ± 8.0 Ma (Fig. 4a). *In situ* laser ablation of white mica in Bay0851 provided scattered isotopic dates that, except for one analysis, are distributed into two groups (Fig. 4b): one *c.* 83.4 ± 0.7 Ma (four analyses) and another one 74.6 ± 1.1 Ma (three analyses). Mineral separates from sample Yah04 yielded well-defined plateaux (Fig. 4a), indicating

Table 3. Composition of individual chlorite and chloritoid and thermobarometric results of chlorite–chloritoid–quartz–water multi-equilibrium calculations in sample Yah04.

	Pair 1		Pair 2		Pair 3		Pair 4		Pair 5		Pair 6		Pair 7	
	Cld	Chl	Cld	Chl	Cld	Chl	Cld	Chl	Cld	Chl	Cld	Chl	Cld	Chl
SiO_2	24.65	25.46	24.43	29.96	24.58	25.11	24.58	25.16	24.80	25.61	25.84	25.93	24.26	25.94
$A1_2O_3$	42.15	25.89	41.99	26.05	41.85	25.88	41.64	25.75	41.63	25.29	39.71	25.54	41.85	25.13
FeO	25.39	23.25	25.19	22.04	25.40	22.52	25.78	22.78	25.32	23.21	24.78	22.23	24.69	22.15
MnO	0.29	0.08	0.23	0.07	0.21	0.00	0.21	0.00	0.33	0.04	0.18	0.02	0.28	0.09
MgO	2.31	14.03	2.56	14.47	2.56	14.92	2.43	14.76	2.34	14.85	3.63	15.47	2.45	15.60
CaO	0.01	0.05	0.00	0.02	0.00	0.02	0.00	0.02	0.00	0.02	0.01	0.02	0.00	0.03
Na_2O	0.00	0.06	0.02	0.04	0.00	0.01	0.00	0.02	0.03	0.02	0.00	0.00	0.01	0.00
K_2O	0.03	0.05	0.00	0.03	0.01	0.04	0.00	0.03	0.01	0.03	0.02	0.03	0.02	0.02
Total	94.83	88.87	94.44	92.67	94.61	88.50	94.64	88.52	94.45	89.07	94.19	89.23	93.57	88.95
Si(Tl + T2)	1.99	2.59	1.98	2.63	1.99	2.55	1.99	2.56	2.01	2.59	2.09	2.58	1.98	2.62
A1(T2)	4.01	1.40	4.01	1.37	3.99	1.45	3.98	1.44	3.97	1.41	3.79	1.42	4.02	1.38
A1(M1)		0.40		0.37		0.45		0.44		0.41		0.42		0.38
Mg(Ml)	0.28	0.23	0.31	0.23	0.31	0.21	0.29	0.22	0.28	0.23	0.44	0.18	0.30	0.26
Fe2 + (M1)	1.71	0.22	1.71	0.20	1.72	0.17	1.75	0.17	1.72	0.19	1.68	0.11	1.68	0.19
V(M1)		0.15		0.20		0.17		0.17		0.17		0.29		0.17
Mg(M2 + M3)		1.90		1.95		2.04		2.05		2.01		2.11		2.09
Fe2 + (M2 + M3)		1.76		1.62		1.60		1.62		1.63		1.30		1.56
A1(M2 + M3)		0.31		0.41		0.35		0.35		0.35		0.58		0.34
A1(M4)		1.00		0.95		0.85		0.85		0.85		0.56		0.88
Fe^{3+}(M4)		0.00		0.05		0.15		0.14		0.15		0.44		0.12
Cln		0.23		0.23		0.21		0.22		0.23		0.18		0.26
Daph		0.22		0.20		0.17		0.17		0.19		0.11		0.19
Am		0.40		0.37		0.45		0.44		0.41		0.42		0.38
Sud		0.15		0.20		0.17		0.17		0.17		0.29		0.17
XMg(Cld)	0.14		0.15		0.15		0.15		0.14		0.22		0.15	
P (GPa)	0.82		0.89		0.95		0.96		0.95		1.13		0.96	
T(°C)	411		400		425		418		400		383		389	

consistent dates of 66.7 ± 0.4 Ma, 65.7 ± 0.2 Ma, and 64.8 ± 0.4 Ma. Each separate, isochron and inverted isochron dates, as well as total gas dates, are similar to these plateau dates within the 2-SD analytical uncertainty (Table S4).

Ören Unit. Mineral separates from the sample Ören001 furnished well-defined plateaux (Fig. 4b), indicating dates of 60.3 ± 0.3 Ma, 62.6 ± 0.4 Ma and 59.4 ± 0.7 Ma. For each separate, isochron and inverted isochron dates, as well as total gas dates, are similar to these plateau dates within the 2-SD analytical uncertainty (Table S4).

Kurudere–Nebiler Unit. *In situ* laser ablation of white mica in Kuru0110 provided isotopic dates scattered from 35.0 ± 2.5 to 88.5 ± 47.1 and 378.4 ± 346.1 Ma. Five of the eight steps, representing ~71% of the total ^{39}Ar release, give an average date of 45.2 ± 2.0 Ma (Fig. 4a). *In situ* laser ablation of white mica in Nebil0101 yielded isotopic dates scattered between 24.2 ± 1.8 and 30.2 ± 2.5 Ma. Five of the seven steps, representing ~56% of the total ^{39}Ar release, give an average date of 26.5 ± 0.8 Ma (Fig. 4a).

INTERPRETATION OF ISOTOPIC DATES

Afyon Zone

In situ laser ablation analysis of white mica in the carpholite-bearing phyllite sample Bay0851 yielded two date trends: *c*. 83 and 75 Ma (Fig. 4b). Due to the fine grain size of phengite in this sample, laser ablation was performed on relatively large areas to extract sufficient gas. Therefore, no link could be established between the composition of phengite analysed and the isotopic results. Owing to this lack of textural control, the dates cannot be interpreted unequivocally.

In all investigated quartz vein samples, phengite, with chlorite, formed at the expanse of carpholite. Accordingly, thermobarometric calculations for samples Afy0206 and Yah04 show that ^{40}Ar–^{39}Ar phengite dates correspond to medium- to low-*P* conditions during retrograde stages of the H*P*–L*T* history. Chlorite–quartz–water temperatures indicate that phengite consistently grow below 400 °C, that is below Ar closure temperature in phengite, assumedly similar to that in muscovite (Wijbrans & McDougall, 1986; Hames & Bowring, 1994; Reddy *et al*., 1996), i.e. ≥ 450–500 °C (e.g. Hammerschmidt & Frank, 1991; Di Vincenzo & Palmeri, 2001; Balogh & Dunkl, 2005; Allaz, 2008). Besides, in samples Afy0212 and Kűt0815, phengite formed in equilibrium with pyrophyllite, i.e. below 400–450 °C. White mica ^{40}Ar–^{39}Ar dates from these samples therefore represent crystallization ages. Therefore, it is inferred that the carpholite-bearing rocks from the Afyon Zone were exhumed through medium pressure (0.6–0.7 GPa) *c*. 65–62 and 67–64 Ma the western and eastern parts of the Afyon Zone respectively. Given that the highest stratigraphic level of the Afyon Zone is represented by a Campanian olistostrom (*c*. 83–70 Ma; Özer & Tansel Öngen, 2012), the metamorphic peak might have occurred only a few million years earlier than the ^{40}Ar–^{39}Ar dates, assumably *c*. 70 Ma.

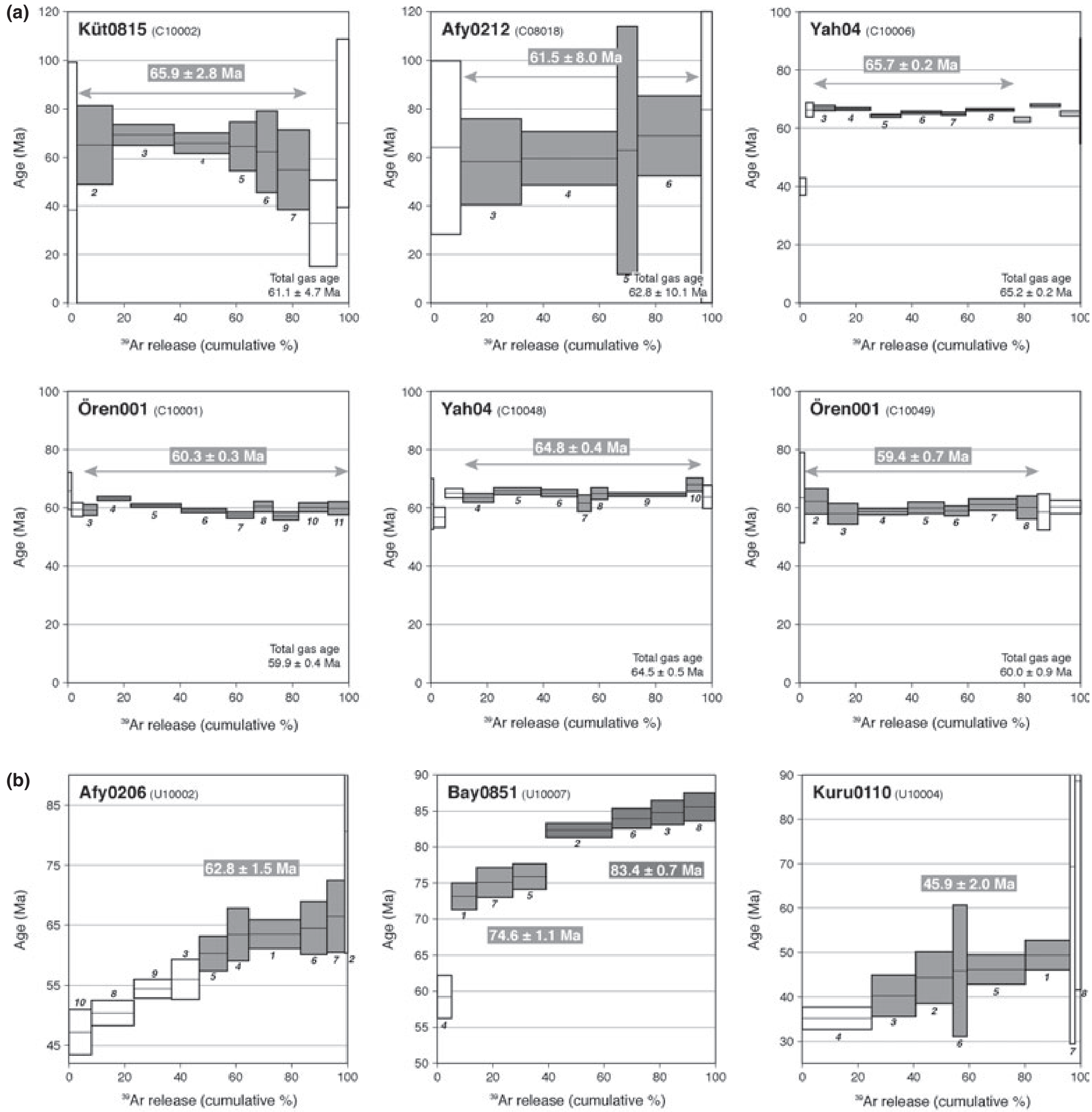

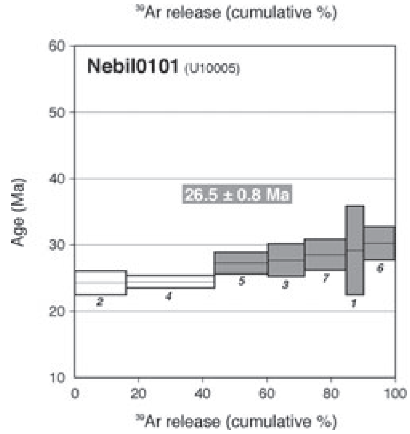

Figure 4. ^{40}Ar–^{39}Ar age spectra. a) Representative plateau date diagrams obtained by stepwise heating of separated grains using a CO_2 laser. b) "Pseudo-plateau" date diagrams for in situ UV-laser ablation of white mica in rock sections. Box numbers refer to step numbers in the Table S4.

Ören Unit

According to the *P–T* estimates of Rimmelé *et al.* (2005), phengite and chlorite from sample Ören001 formed between 1.1 GPa/400 °C (interpreted as near-peak conditions) and 0.8 GPa/300 °C, depicting a syn-decompression cooling path. Again, phengite in this sample formed below Ar closure temperature, so ^{40}Ar–^{39}Ar dates represent mineral growth. Hence, 63–59 Ma ^{40}Ar–^{39}Ar dates obtained for sample Ören001 correspond to early H*P*–L*T* retrograde stages in the Ören Unit.

Kurudere–Nebiler Unit

Previous studies estimated that carpholite-bearing rocks from this units experienced temperatures up to 450–500 °C (Rimmelé *et al.*, 2005; Whitney *et al.*, 2008). In samples Kuru0110 and Nebil0101, Ar isotopic system might therefore have been partially to completely reset. Unambiguous textures in Kuru0110 display that white mica formed coevally with chlorite and kyanite from the breakdown of carpholite (only preserved as tiny fibres in quartz), that is during early retrograde metamorphism (Rimmelé *et al.*, 2005). The partial preservation of diaspore in metabauxites in the area of Kurudere suggests that this part of the unit was not affected by a significant thermal overprint during its exhumation (Fig. 5; Rimmelé *et al.*, 2005). In other words, Ar closure temperature may have not been attained, so that phengite formed during post-H*P* decompression preserved its initial Ar ratio signature. The mean ^{40}Ar–^{39}Ar date of 45.2 ± 2.0 Ma obtained from this sample probably represents early H*P* retrograde stages.

In sample Nebil0101, phengite defines a post-kyanite and -chloritoid foliation, and therefore represents later metamorphic stages than that in Kuru0110. The lack, in this area, of relicts of carpholite (entirely replaced by chlorite and kyanite) and diaspore (entirely replaced by corundum), is regarded as the result of more intense thermal overprint at low-to-medium pressure as compared with the area of Kurudere. The average ^{40}Ar–^{39}Ar date (26.5 ± 0.8 Ma) obtained for Nebil0101 might hence represent cooling below Ar closure temperature following the Barrovian-type metamorphism.

The contrasting dates obtained from the two dated localities of the Kurudere–Nebiler Unit therefore are inferred to represent two distinct metamorphic stages (Fig. 5).

DISCUSSION

Tectonic implications

The new data indicate that the Ören Unit and the Afyon Zone were exhumed from H*P*–L*T* conditions synchronously (retrogression *c.* 65–60 Ma). Both units underwent similar metamorphic conditions restricted to < 400–450 °C. Although some parts of the Ören Unit followed a syn-cooling decompression path (Rimmelé *et al.*, 2005), others obviously experienced relatively isothermal decompression, engendering partial to complete retrogression of carpholite into chlorite, as also evidenced in the Afyon Zone (this study). The Ören Unit and Afyon Zone therefore share a common and coeval metamorphic history (Fig. 5).

These units can be further compared on the basis of structural, kinematic, and stratigraphic data: (i) the contact between the Ören Unit and the Afyon Zone does not crop out anywhere. Both units have similar structural positions regarding the adjacent tectonic units: they lie over the Menderes Nappes and the Cycladic Blueschist Unit, and below the ophiolites and associated mélange emplaced on top of the Anatolide–Tauride units (Fig. 1); (ii) after restoration of the Neogene scissor-like extensional tectonics (e.g. Gessner *et al.*, 2001b; van Hinsbergen, 2010; Pourteau *et al.*, 2010), shear indicators documented along the original basal thrust and in the lower schists of the Ören Unit (Rimmelé *et al.*, 2003a, 2006) point to top-to-ESE transport of the Ören Unit over the Menderes Nappes (e.g. van Hinsbergen, 2010). The Ören Unit can thus be restored to the northwestern margin of the Menderes Nappes, in the same structural position as the Afyon Zone; and (iii) the lithostratigraphy of the Ören Unit is similar to that of Mesozoic series of the western Afyon Zone (e.g. Candan *et al.*, 2005; Pourteau *et al.*, 2010). Especially, reddish metasedimentary rocks containing carpholite-bearing quartz veins characteristic of the Ören Unit (Rimmelé *et al.*, 2003a) are also typical of the Kütahya area, in the western Afyon Zone (Pourteau *et al.*, 2010).

Based on these metamorphic, geochronological, structural, kinematic and stratigraphic criteria, it is proposed that, before the Ören Unit was transported on top of the Menderes Massif, it represented the western continuation of the Afyon Zone. These units are thus merged as the Ören-Afyon Zone, which represents a Maastrichtian H*P*–L*T* metamorphic belt continuous (before extensional tectonics started in Western Anatolia) from the Aegean Coast to Central Anatolia, i.e. over more than 700 km. Interestingly, no lateral equivalent towards Eastern Anatolia and in Aegea is known yet.

On the other hand, the Kurudere–Nebiler Unit experienced H*P*–L*T* metamorphism coevally with the Cycladic Blueschist Unit, i.e. in the early Eocene (e.g. Jolivet & Brun, 2008; Ring *et al.*, 2010). Owing to differences in rock type and *P–T* conditions, the Kurudere–Nebiler Unit and the Cycladic Blueschist Unit cannot be considered a single tectonic unit. Instead, they form a continuous, internally imbricated, Eocene H*P*–L*T* metamorphic belt, clearly distinct from the overlying Ören–Afyon Zone. To

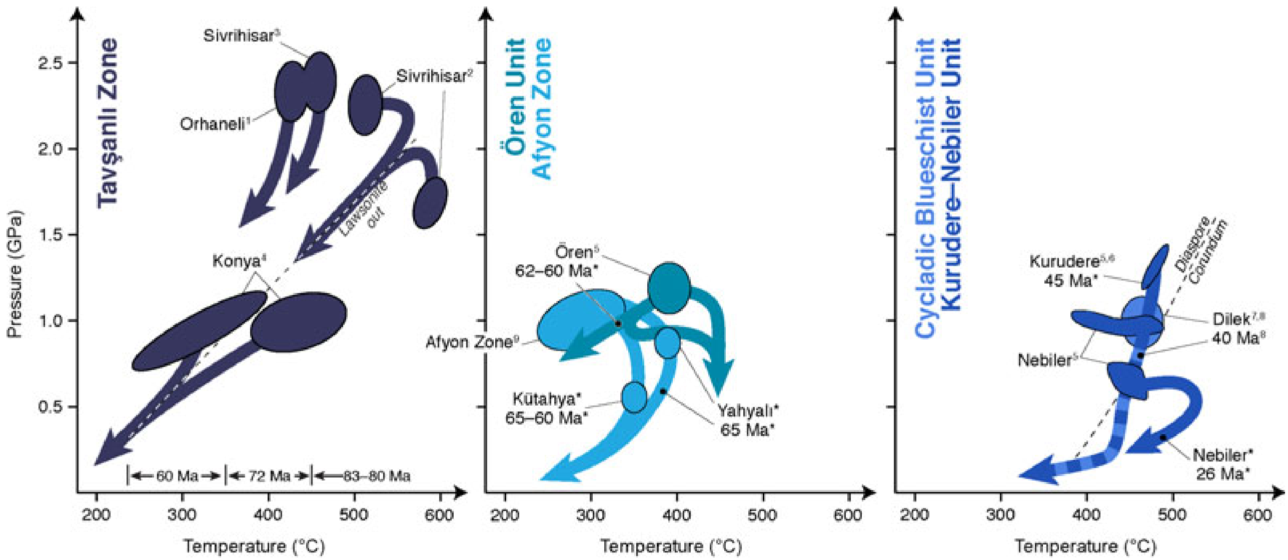

Figure 5. Synthetic peak- to retrograde *P–T–t* paths for the three Anatolide H*P* metamorphic belts. Superscript label refers to references: 1, Okay *et al.* (1998), Okay (2002); 2, Davis & Whitney (2006, 2008); 3, Çetinkaplan *et al.* (2008); 4, Droop *et al.* (2005); 5, Rimmelé *et al.* (2005); 6, Rimmelé *et al.* (2003b); 7, Candan *et al.* (1997); 8, Oberhänsli *et al.* (1998); 9, Pourteau (2011); *, this study. Note that for the region of Sivrihisar (Tavşanlı Zone), only three representative paths are shown among those available in the cited literature (Davis & Whitney, 2006, 2008; Çetinkaplan *et al.*, 2008). Time intervals for the Tavşanlı Zone are phengite ^{87}Rb–^{86}Sr dates from Sherlock *et al.* (1999) as compiled by Davis (2011).

explain the *c.* 20 Ma gap between the H*P*–L*T* metamorphism in the Ören–Afyon Zone (*c.* 70–65 Ma) and the Kurudere–Nebiler and Cycladic Blueschist Units (52–45 Ma), these domains might have been once separated by a narrow basin correlating with the Pindos Basin (e.g. Jolivet *et al.*, 2004; Papanikolaou, 2009), also referred to as the Selçuk Ocean (Gessner *et al.*, 2001c). In Western Anatolia, the Tavşanlı and Ören–Afyon Zones represent the exhumed part of a deeply buried microcontinent distinct from the southern Cycladic–Menderes–Tauride microcontinent (Fig. 6). Whether the Pindos Basin was floored by oceanic or thinned continental crust remains an unresolved issue and is out of the scope of this study. Nevertheless, the oceanic-floor idea is supported by the occurrence of oceanic material in the metamorphosed mélange unit (blocks of eclogitic Late Cretaceous metabasalts and metagabbros, as well as meta-serpentinite; Bröcker & Enders, 2001; Gessner *et al.*, 2001c; Çetinkaplan, 2002; Bulle *et al.*, 2010), and tectonic lenses of serpentinite intercalated between the Ören Unit and the Cycladic Blueschist Unit or Kurudere–Nebiler Unit (Rimmelé *et al.*, 2003a). The northward subduction of negatively buoyant oceanic crust underneath the Tavşanlı and Ören–Afyon Zones constitutes the most likely explanation for: (i) deep burial to H*P*–L*P* conditions and subsequent exhumation of the Kurudere–Nabiler and Cycladic Blueschist Units; and (ii) contemporarily, mantle melting beneath the Tavşanlı Zone (early Eocene plutons; Harris *et al.*, 1994). The absence of any Eocene H*P*–L*T* metamorphic rocks and calc-alkaline plutons towards Central Anatolia indicates that the Pindos Ocean did not extend so far east.

In consequence, Western Anatolia encloses three H*P*–L*T* metamorphic units that are successively younger from top to bottom, and from the internals towards the externals of the convergence belt. The metamorphic evolution of these units can be compared with each other on the basis of the *P–T–t* paths presented in Fig. 5. Complex palaeogeography and tectonic development of Western Anatolia are comparable to those of the Western Alps (e.g. Schmid *et al.*, 2004), the Aegean Domain (van Hinsbergen *et al.*, 2005; Jolivet & Brun, 2008; Papanikolaou, 2009) and the Himalaya (van Hinsbergen *et al.*, 2012), where distinct continental fragments separated by thinned continental- or oceanic crust domains were successively accreted, buried deeply, and exhumed in a context of continuous subduction. Following this model of outward trench migration, northward subduction between the Pontides and the Taurides is assumed to have been continuous between 90 and 60 Ma in Central Anatolia, and between 90 and *c.* 30 Ma in Western Anatolia.

Geodynamic evolution of Central Anatolia

The continental-accretion history of Central Anatolia is reconstructed as follows:

93–90 Ma: Onset of intra-oceanic subduction (e.g. Dilek *et al.*, 1999; Parlak & Delaloye, 1999);

88–78 Ma: H*P*–L*T* metamorphism and onset of the exhumation of the deeply buried, distal part of the Anatolide–Tauride passive continental margin

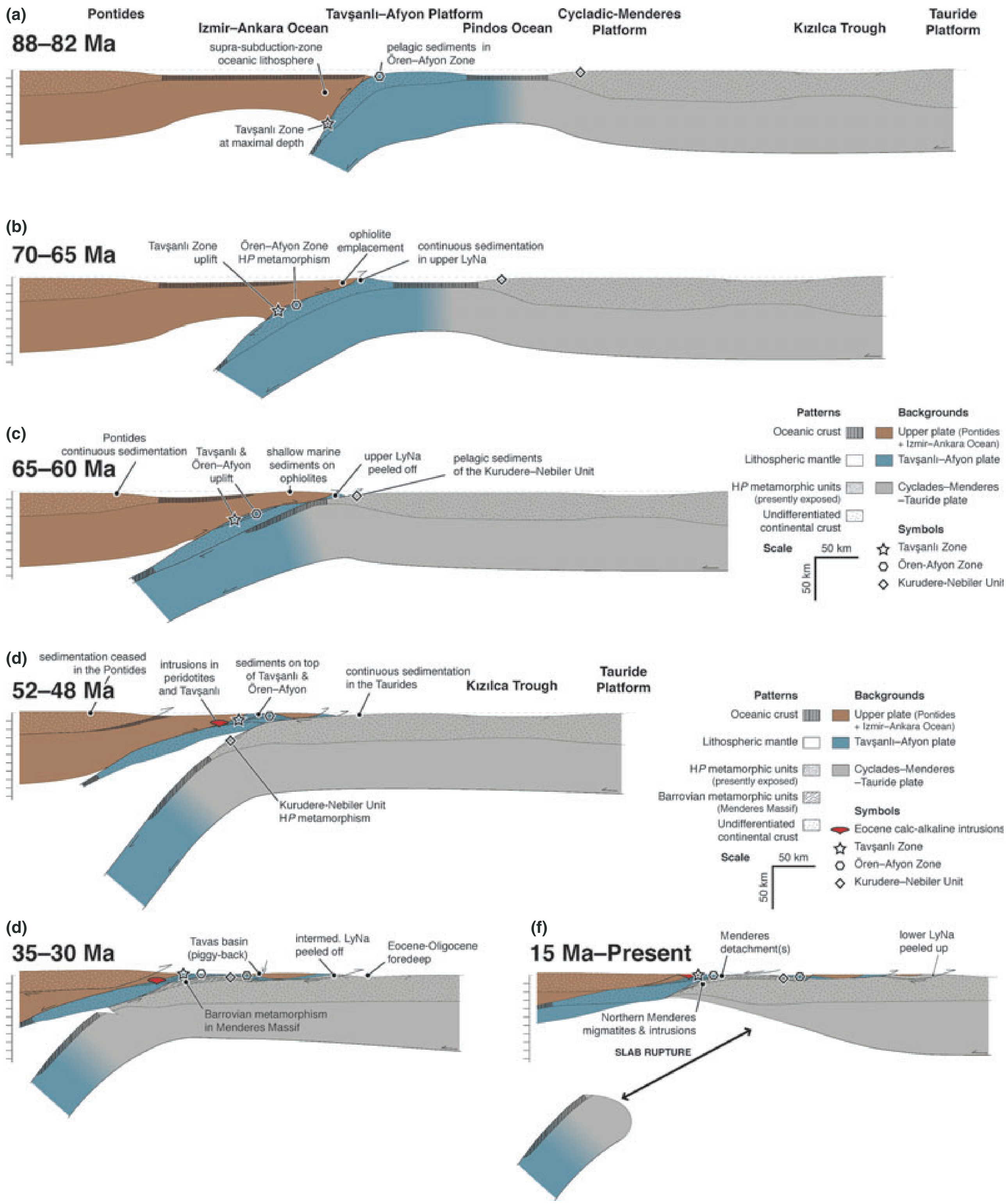

Figure 6. Lithospheric-scale schematic reconstruction of the geodynamic evolution of western Anatolia from the Late Cretaceous to the Neogene.

(Tavşanlı Zone) (assuming similar dates to the western part of the unit; e.g. Sherlock *et al.*, 1999; Seaton *et al.*, 2009), coevally with arc magmatism, Barrovian-type metamorphism and core complex formation in the Central Anatolian Crystalline Complex (e.g. Whitney *et al.*, 2003, 2007; Gautier *et al.*, 2008; Lefebvre *et al.*, 2011);

75–65 Ma: Exhumation of the Tavşanlı Zone up to Moho depths, coevally with the burial of more proximal parts of the margin (Afyon Zone; this study);

65–60 Ma: Exhumation of both HP–LT units (this study) possibly during a continental collision stage (Seaton *et al.*, 2009; Whitney *et al.*, 2011), and emplacement of ophiolites on external platform units (Central and Eastern Taurides; Fig. 1) (e.g. Dilek *et al.*, 1999);

55 Ma and later: Marine sedimentation and calk-alkaline magmatism sealing the suture zone (Görür *et al.*, 1998; Clark & Robertson, 2002).

After the cessation of subduction in the earliest Cenozoic, continuous north–south convergence between Central Anatolia and Northeastern Africa was accommodated along the Cyprus trench.

Geodynamic evolution of Western Anatolia

Western Anatolia encompasses three HP–LT metamorphic units: the Tavşanlı Zone buried to 50–80 km *c.* 88–82 Ma, the Ören–Afyon Zone buried to 30–45 km *c.* 70–65 Ma, and the Kurudere–Nebiler Unit, connected westwards to the Cycladic Blueschist Unit, buried to 30–50 km *c.* 52–45 Ma. Hereafter, a geodynamic scenario for Western Anatolia (Fig. 6) is proposed, accounting for the contrasting P–T–t loops followed by these three successive HP belts (Fig. 5).

From 95 to 75 Ma

North-dipping intra-oceanic subduction started between the Anatolide–Tauride Block and the Pontides *c.* 93–90 Ma (Robertson, 2002; Çelik *et al.*, 2006). Around 85 Ma, that is, shortly after subduction initiation, the rocks of the Tavşanlı Zone, representing the most distal parts of a continental passive margin, attained the deepest burial levels (*c.* 70–80 Ma; Okay *et al.*, 1998; Sherlock *et al.*, 1999; Okay, 2002; Davis & Whitney, 2006). In this period, sedimentation persisted in the more external units, i.e. the Afyon Zone, the Kurudere–Nebiler Unit and the Taurides (Fig. 6a) (Candan *et al.*, 2005).

Then, blueschists and eclogites of the Tavşanlı Zone were exhumed along a very-low apparent geothermal gradient, accounting for the good preservation of lawsonite along the retrograde path (Whitney & Davis, 2006). Such syn-decompression cooling is evidence for mid-speed to slow exhumation during continuous subduction (e.g. Ernst, 1988; Liou *et al.*, 1994), i.e. during the underplating of the Afyon Zone.

From 75 to 55 Ma

The Ören–Afyon Zone, including a carbonate platform and its Precambrian–Palaeozoic substratum, was metamorphosed under low-grade HP conditions at *c.* 70 Ma, while the carbonate platform of the Kurudere–Nebiler Unit recorded subsidence from neritic to pelagic environments (Candan *et al.*, 2005). The Ören–Afyon and the Tavşanlı Zones were then exhumed synchronously up to shallow crustal levels from Maastrichtian to Palaeocene times. Coevally, the ophiolites from the Izmir–Ankara and Inner-Tauride oceanic branches were emplaced southwards on top of Mesozoic platform sediments (Okay *et al.*, 2001), initiating the formation of the Tauride nappe complexes (e.g. Collins & Robertson, 1998; Elitok & Drüppel, 2008).

In Western Anatolia, the active trench was transferred southwards within the Pindos Ocean sometime around the early Palaeocene (*c.* 65–60 Ma) due to continuous regional convergence. It can be envisaged that the southward migration of the subduction zone was accommodated by decoupling along either a weak surface separating the upper–middle from the lower crust (Jolivet *et al.*, 2003), or the crust–mantle interface ('tectonic Moho').

From 55 to 35 Ma

The northward subduction in the Pindos Ocean was accompanied by melting in the overlying mantle wedge, resulting in the intrusion of calc-alkaline magmas in the overriding Tavşanlı Zone and Western Pontides (Harris *et al.*, 1994; Delaloye & Bingol, 2000). In this period, while some parts of the Tavşanlı Zone were still at a depth of ~10 km (Harris *et al.*, 1994), others, as well as the Afyon Zone, were already exposed at the surface and unconformably covered by shallow-marine sedimentary rocks (Özcan *et al.*, 1988).

Coevally, the Kurudere–Nebiler Unit, representing the northern edge of the Menderes–Tauride platform, was dragged down to HP–LT conditions and subsequently exhumed from the middle Eocene on. This correlates with a second imbrication stage in the Tauride nappe complexes (incorporation of Eocene and older platform sequences; e.g. Collins & Robertson, 1998).

From 35 Ma onwards

Around the Eocene–Oligocene boundary, the collision of the Menderes–Tauride platform and the overlying terranes, as recorded by Barrovian metamorphism in the Menderes Massif *sensu lato* (Bozkurt & Oberhänsli, 2001; Gessner *et al.*, 2001a; Régnier *et al.*, 2003), attained an orogenic stage characterized by a regional sedimentary hiatus and local molasse-type sedimentation in the Taurides (e.g. Şengör *et al.*, 1984; Yılmaz *et al.*, 2000; MTA, 2002). Continental collision was followed by the unroofing of the Menderes Nappes along detachment faults in the Miocene (e.g. Hetzel *et al.*, 1995; Gessner *et al.*, 2001b), due to slab roll-back. Shortening, however, persisted in the Taurides, leading to the final emplacement of the Lycian Nappes onto lower-middle Miocene foredeep sedimentary rocks and the autochthonous platform (Gutnic *et al.*, 1979; Collins & Robertson, 1998).

The Oligo–Miocene H*P* belt of the Aegean Domain (in Crete and the Pelopponesus; e.g. Theye *et al*., 1992) is evidence that subduction continued in the Aegean Domain, whereas it ceased below Western Anatolia, where no equivalent metamorphic unit is exposed. In the same way, given the interruption of the early Eocene H*P* belt east to the Menderes Massif *s.l.*, the Inner Tauride subduction system of Central Anatolia was blocked after the accretion of the Tavşanlı–Afyon units at *c*. 65 Ma.

Continuation (as in Aegea) *v* cessation (as in Anatolia) of subduction is probably controlled by the possibility of tectonic decoupling between the accreted, buoyant continental crust and the underlying, dense lithospheric mantle, and might thus depend on palaeogeography (i.e. size of the accreted microcontinent). Consequently, continental collision in Central and Western Anatolia is assumed to have engendered locking of the subduction in the earliest Cenozoic and the Oligocene, respectively. In the Oligocene to early Miocene, the increasing curvature of the retreating Hellenic subduction zone led to tearing along the eastern limb of the slab, i.e. below Southwestern Anatolia (Dilek & Altunkaynak, 2009; van Hinsbergen *et al*., 2010).

CONCLUSIONS

This study presents the first results of phengite ^{40}Ar–^{39}Ar geochronology and chlorite–phengite multi-equilibrium thermobarometry on Fe-Mg-carpholite-bearing rocks from three tectonic units of Western and Central Anatolia, and discusses the tectonic relations between them. The exhumation of the Afyon Zone through greenschist-facies conditions was dated to 67–62 Ma, and earliest retrograde stages in the Ören Unit to 63–59 Ma. Consequently, the Ören Unit is considered the western continuation of the Afyon Zone until extensional tectonics led to its transport away from the suture zone. The Kurudere–Nebiler Unit (Mesozoic cover of the southern Menderes Massif) was retrogressed under greenschist-facies conditions *c*. 46 Ma, subsequently affected by a Barrovian overprint (likely *c*. 40–35 Ma) and cooled below ~450–500 °C at *c*. 26 Ma. The Kurudere–Nebiler Unit correlates with the Cycladic Blueschist Unit, which experienced a similar, synchronous metamorphic evolution. These units represent parts of an Eocene H*P*–L*T* belt resulting from the entrance of the Menderes–Tauride microcontinent in the Pindos subduction zone.

This study shows that by combining isotopic geochronology and thermobarometric calculations in individual samples, specific *P*–*T* conditions can be ascribed to isotopic dates, which can thus be deciphered with a greater accuracy to compare the evolution of metamorphic rocks at regional scales. Based on the lateral continuation or interruption of the Anatolian H*P*–L*T* metamorphic belts, it is argued that subduction was blocked earlier in Central Anatolia (earliest Cenozoic) than in Western Anatolia (Oligocene), while it still is active in the Aegean Domain.

ACKNOWLEDGEMENTS

Financial support by the Deutsche Forschungsgemeinschaft (OB80/34) is kindly acknowledged. S. Schmid, G. Salaün, M. Handy, and R. Bousquet are thanked for fruitful discussions on the early versions of this manuscript. D. Whitney (ed.), L. Webb, and two anonymous reviewers are also thanked for their constructive comments.

REFERENCES

Agard, P., Vidal, O. & Goffé, B., 2001. Interlayer and Si content of phengite in HP-LT carpholite-bearing metapelites. *Journal of Metamorphic Geology*, **19,** 477–493.

Agard, P., Monié, P., Jolivet, L. & Goffé, B., 2002. Exhumation of the Schistes Lustrés complex: *in situ* laser probe ^{40}Ar/^{39}Ar constraints and implications for the Western Alps. *Journal of Metamorphic Geology*, **20,** 599–618.

Akal, C., Candan, O., Koralay, E., Oberhänsli, R., Chen, F. & Prelevic, D., 2012. Early Triassic potassic volcanism in the Afyon Zone of the Anatolides/Turkey: implications for the rifting of the Neo-Tethys. *International Journal of Earth Sciences* **101,** 177–194.

Allaz, J., 2008. Metamorphic evolution of the Central Alps: linking ^{39}Ar-^{40}Ar dating with thermobarometry, PhD thesis, Universität Bern, Switzerland.

Altiner, D., Koçyiğit, A., Farinacci, A., Nicosia, U. & Conti, M.A., 1991. Jurassic-Lower Cretaceous stratigraphy and paleogeographic evolution of the southern part of north-western Anatolia. *Geologica Romana*, **27,** 13–80.

Arkai, P., Faryad, S.W., Vidal, O. & Balogh, K., 2003. Very low-grade metamorphism of sedimentary rocks of the Meliata unit, Western Carpathians, Slovakia: implications of phyllosilicate characteristics. *International Journal of Earth Sciences*, **92,** 68–85.

Aydın, N.S., Göncüoğlu, M.C. & Erler, A., 1998. Latest Cretaceous magmatism in the central Anatolian crystalline complex: review of field, petrographic and geochemical features. *Turkish Journal of Earth Sciences*, **7,** 259–268.

Azañon, J.M. & Goffé, B., 1997. Ferro- and magnesiocarpholite assemblages as record of high-P, low T metamorphism in the Central Alpujarrides, Betic cordillera (SE Spain). *European Journal of Mineralogy*, **9,** 1035–1051.

Balogh, K. & Dunkl, I., 2005. Argon and fission track dating of Alpine metamorphism and basement exhumation in the Sopron Mts. (Eastern Alps, Hungary): thermochronology or mineral growth? *Mineralogy and Petrology*, **83,** 191–218.

Berman, R.G., 1988. Internally-consistent thermodynamic data for minerals in the system Na_2O-K_2O-Ca-MgO-FeO-Fe_2O_3-Al_2O_3-SiO_2-TiO_2-H_2O-CO_2. *Journal of Petrology*, **29,** 445–522.

Bijwaard, H., Spakman, W. & Engdahl, E.R., 1998. Closing the gap between regional and global travel time tomography. *Journal of Geophysical Research-Solid Earth*, **103,** 30055–30078.

Biryol, C.B., Beck, S.L., Zandt, G. & Ozacar, A.A., 2011. Segmented African lithosphere beneath the Anatolian region inferred from teleseismic P-wave tomography. *Geophysical Journal International*, **184,** 1037–1057.

Bousquet, R., Oberhänsli, R., Goffé, B., Jolivet, L. & Vidal, O., 1998. High pressure-low temperature metamorphism and deformation in the Bündnerschiefer of the Engadine window: implications for the regional evolution of the eastern Central Alps. *Journal of Metamorphic Geology*, **16,** 657–674.

Bousquet, R., Goffé, B., Vidal, O., Oberhänsli, R. & Patriat, M., 2002. The tectono-metamorphic history of the Valaisan domain from the Western to the Central Alps: new constraints for the evolution of the Alps. *Bulletin of the Geological Society of America*, **114,** 207–225.

Bozkurt, E. & Oberhänsli, R., 2001. Menderes Massif (Western Turkey): structural, metamorphic and magmatic evolution – a synthesis. *International Journal of Earth Sciences*, **89,** 679–708.

Bozkurt, E. & Satır, M., 2000. The southern Menderes Massif (western Turkey): geochronology and exhumation history. *Geological Journal*, **35,** 285–296.

Bröcker, M. & Enders, M., 2001. Unusual bulk-rock compositions in eclogite-facies rocks from Syros and Tinos (Cyclades, Greece): implications for U-Pb zircon geochronology. *Chemical Geology*, **175,** 581–603.

Bulle, F., Bröcker, M., Gaertner, C. & Keasling, A., 2010. Geochemistry and geochronology of HP melanges from Tinos and Andros, cycladic blueschist belt, Greece. *Lithos*, **117,** 61–81.

Candan, O., Dora, O.Ö., Oberhänsi, R., Oelsner, F. & Dürr, S., 1997. Blueschist relics in the Mesozoic cover series of the Menderes Massif and correlations with Samos Islan, Cyclades. *Schweizerische Mineralogische und Petrographische Mitteilungen*, **77,** 95–99.

Candan, O., Çetinkaplan, M., Oberhänsli, R., Rimmelé, G. & Akal, C., 2005. Alpine high-P/low-T metamorphism of the Afyon Zone and implications for the metamorphic evolution of Western Anatolia, Turkey. *Lithos*, **84,** 102–124.

Candan, O., Oberhänsli, R., Dora, O.Ö. *et al*., 2011. Polymetamorphic evolution of the Pan-African basement and Palaeozoic-Early Tertiary cover series of the Menderes Massif. *Bulletin of the Mineral Research and Exploration Institute of Turkey*, **142,** 121–163.

Cathelineau, M. & Nieva, D., 1985. A chlorite solid-solution geothermometer – the Los-Azufres (Mexico) geothermal system. *Contributions to Mineralogy and Petrology*, **91,** 235–244.

Çelik, Ö.F., Delaloye, M. & Feraud, G., 2006. Precise Ar-40-Ar-39 ages from the metamorphic sole rocks of the Tauride Belt Ophiolites, southern Turkey: implications for the rapid cooling history. *Geological Magazine*, **143,** 213–227.

Çetinkaplan, M., 2002. Tertiary High-Pressure/Low-Temperature Metamorphism in the Mesozoic Cover Series of the Menderes Massif and Correlation with the Cycladic Crystalline Complex. Unpublished PhD thesis, Universitesi Izmir.

Çetinkaplan, M., Candan, O., Oberhänsli, R. & Bousquet, R., 2008. Pressure-temperature evolution of lawsonite eclogite in Sivriihisar; Tavsanli Zone-Turkey. *Lithos*, **104,** 12–32.

Chopin, C. & Schreyer, W., 1983. Magnesiocarpholite and magnesiochloritoid: two index minerals of pelitic blueschists and their preliminary phase relations in the system MgO-Al_2O_3-SiO_2-H_2O. *American Journal of Science*, **283-A,** 72–96.

Clark, M. & Robertson, A.H.F., 2002. The role of the Early Tertiary Ulukişla Basin, southern Turkey, in suturing of the Mesozoic Tethys ocean. *Journal of the Geological Society, London*, **159,** 673–690.

Collins, A.S. & Robertson, A.H.F., 1998. Processes of Late Cretaceous to Late Miocene episodic thrust-sheet translation in the Lycian Taurides, SW Turkey. *Journal of the Geological Society, London*, **155,** 759–772.

Davis, P.B., 2011. Petrotectonics of lawsonite eclogite exhumation: insights from the Sivrihisar massif, Turkey. *Tectonics*, **30,** TC1006.

Davis, P.B. & Whitney, D.L., 2006. Petrogenesis of lawsonite and epidote eclogite and blueschist, Sivrihisar Massif, Turkey. *Journal of Metamorphic Geology*, **24,** 823–849.

Davis, P.B. & Whitney, D.L., 2008. Petrogenesis and structural petrology of high-pressure metabasalt pods, Sivrihisar, Turkey. *Contributions to Mineralogy and Petrology*, **156,** 217–241.

De Andrade, V., Vidal, O., Lewin, E., O'Brien, P. & Agard, P., 2006. Quantification of electron microprobe compositional maps of rock thin sections: an optimized method and examples. *Journal of Metamorphic Geology*, **24,** 655–668.

De Capitani, C. & Petrakakis, K., 2010. The computation of equilibrium assemblage diagrams with Theriak/Domino software. *American Mineralogist*, **95,** 1006–1016.

Delaloye, M. & Bingol, E., 2000. Granitoids from Western and Northwestern Anatolia: geochemistry and modeling of geodynamic evolution. *International Geology Review*, **42,** 241–268.

Di Vincenzo, G. & Palmeri, R., 2001. An ^{40}Ar-^{39}Ar investigation of high-pressure metamorphism and the retrogressive history of mafic eclogites from the Lanterman Range (Antarctica): evidence against a simple temperature control on argon transport in amphibole. *Contributions to Mineralogy and Petrology*, **141,** 15–35.

Dilek, Y. & Altunkaynak, S., 2009. Geochemical and temporal evolution of Cenozoic magmatism in western Turkey: mantle response to collision, slab break-off, and lithospheric tearing in an orogenic belt. In: *Collision and Collapse at the Africa–Arabia–Eurasia Subduction Zone*, Vol. **311** (eds van Hinsbergen, D.J.J., Edwards, M.A. & Govers, R.), pp. 213–233. *Geological Society, London, Special Publications*.

Dilek, Y., Thy, P., Hacker, B. & Grundvig, S., 1999. Structure and petrology of Tauride ophiolites and mafic dike intrusions (Turkey): implications for the Neotethyan ocean. *Bulletin of the Geological Society of America*, **111,** 1192–1216.

Dirik, K., Göncüoğlu, M.C. & Kozlu, H., 1999. Stratigraphy and pre-Miocene tectonic evolution of the southwestern part of the Sivas Basin, Central Anatolia, Turkey. *Geological Journal*, **34,** 303–319.

Droop, G.T.R., Karakaya, M.Q., Eren, Y. & Karakaya, N., 2005. Metamorphic evolution of blueschists of the Altinekin Complex, Konya area, south central Turkey. *Geological Journal*, **40,** 127–153.

Dubacq, B., Vidal, O. & De Andrade, V., 2010. Dehydration of dioctahedral aluminous phyllosilicates: thermodynamic modelling and implications for thermobarometric estimates. *Contributions to Mineralogy and Petrology*, **159,** 159–174.

Dürr, S., 1975. *Über Alter und geotektonische Stellung des Menderes-Kristallins/SW-Anatolien und seine Äquivalente in der mittleren Aegaeis*. Unpub Habilitation Thesis, University of Marburg, Lahn.

Elitok, O. & Drüppel, K., 2008. Geochemistry and tectonic significance of metamorphic sole rocks beneath the Beysehir-Hoyran ophiolite (SW-Turkey). *Lithos*, **100,** 322–353.

Ernst, W.G., 1988. Tectonic history of subduction zones inferred from retrograde blueschist p-t paths. *Geology*, **16,** 1081–1084.

Ganne, J., De Andrade, V., Weinberg, R.F. *et al*., 2012. Modern-style plate subduction preserved in the Palaeoproterozoic West African craton. *Nature Geoscience*, **5,** 60–65.

Gautier, P., Bozkurt, E., Bosse, V., Hallot, E. & Dirik, K., 2008. Coeval extensional shearing and lateral underflow during Late Cretaceous core complex development in the Nigde Massif, Central Anatolia, Turkey. *Tectonics*, **27,** TC 1003.

Gessner, K., Piazolo, S., Güngör, T., Ring, U., Kröner, A. & Passchier, C.W., 2001a. Tectonic significance of deformation patterns in granitoid rocks of the Menderes nappes, Anatolide belt, southwest Turkey. *International Journal of Earth Sciences*, **89,** 766–780.

Gessner, K., Ring, U., Johnson, C., Hetzel, R., Passchier, C.W. & Güngör, T., 2001b. An active bivergent rolling-hinge detachment system: Central Menderes metamorphic core complex in western Turkey. *Geology*, **29,** 611–614.

Gessner, K., Ring, U., Passchier, C.W. & Güngör, T., 2001c. How to resist subduction: evidence for large-scale out-of-sequence thrusting during Eocene collision in western Turkey. *Journal of the Geological Society, London*, **158,** 769–784.

Göncüoğlu, M.C., Dirik, K. & Kozlu, H., 1997. General Characteristics of pre-Alpine and Alpine Terranes in Turkey: explanatory notes to the terrane map of Turkey. *Annales Géologiques des Pays Helleniques*, **37,** 515–536.

Görür, N., Tüysüz, O. & Şengör, A.M.C., 1998. Tectonic Evolution of the Central Anatolian Basins. *International Geology Review*, **40,** 831–850.
Govers, R. & Wortel, M.J.R., 2005. Lithosphere tearing at STEP faults: response to edges of subduction zones. *Earth and Planetary Science Letters*, **236,** 505–523.
Grosch, E.G., Vidal, O., Abu-Alam, T. & McLoughlin, N., 2012. P-T Constraints on the Metamorphic Evolution of the Paleoarchean Kromberg Type-Section, Barberton Greenstone Belt, South Africa. *Journal of Petrology*, **53,** 513–545.
Gutnic, M., Monod, O., Poisson, A. & Dumont, J.-F., 1979. *Géologie des Taurides occidentales (Turquie)*. Société Géologiques de France, Paris.
Hames, W.E. & Bowring, S.A., 1994. An empirical-evaluation of the argon diffusion geometry in muscovite. *Earth and Planetary Science Letters*, **124,** 161–167.
Hammerschmidt, K. & Frank, E., 1991. Relics of high-pressure metamorphism in the Lepontinde Alps (Switzerland) - $^{40}Ar/^{39}Ar$ and microprobe analyses on white K-micas. *Schweizerische Mineralogische und Petrographische Mitteilungen*, **71,** 261–274.
Harris, N.B.W., Kelley, S. & Okay, A.I., 1994. Postcollision Magmatism and Tectonics in Northwest Anatolia. *Contributions to Mineralogy and Petrology*, **117,** 241–252.
Hetzel, R., Passchier, C.W., Ring, U. & Dora, O.Ö., 1995. Bivergent Extension in Orogenic Belts - the Menderes Massif (Southwestern Turkey). *Geology*, **23,** 455–458.
Hillier, S. & Velde, B., 1991. Octahedral occupancy and the chemical-composition of diagenetic (low-temperature) chlorites. *Clay Minerals*, **26,** 149–168.
van Hinsbergen, D.J.J., 2010. A key extensional metamorphic complex reviewed and restored: the Menderes Massif of western Turkey. *Earth-Science Reviews*, **102,** 60–76.
van Hinsbergen, D.J.J., Hafkenscheid, E., Spakman, W., Meulenkamp, J.E. & Wortel, R., 2005. Nappe stacking resulting from subduction of oceanic and continental lithosphere below Greece. *Geology*, **33,** 325–328.
van Hinsbergen, D.J.J., Kaymakci, N., Spakman, W. & Torsvik, T.H., 2010. Reconciling the geological history of western Turkey with plate circuits and mantle tomography. *Earth and Planetary Science Letters*, **297,** 674–686.
van Hinsbergen, D.J.J., Lippert, P.C., Dupont-Nivet, G. *et al*., 2012. Greater India Basin hypothesis and a two-stage Cenozoic collision between India and Asia. *Proceedings of the National Academy of Sciences of the United States of America*, **109,** 7659–7664.
Hsui, A.T. & Youngquist, S., 1985. A dynamic-model of the curvature of the Mariana trench. *Nature*, **318,** 455–457.
Husson, L., Brun, J.-P., Yamato, P. & Faccenna, C., 2009. Episodic slab rollback fosters exhumation of HP-UHP rocks. *Geophysical Journal International*, **179,** 1292–1300.
Ilbeyli, N., Pearce, J.A., Thirlwall, M.F. & Mitchell, J.G., 2004. Petrogenesis of collision-related plutonics in Central Anatolia, Turkey. *Lithos*, **72,** 163–182.
Jolivet, L. & Brun, J.-P., 2008. Cenozoic geodynamic evolution of the Aegean. *International Journal of Earth Sciences*, **99,** 109–138.
Jolivet, L. & Faccenna, C., 2000. Mediterranean extension and the Africa-Eurasia collision. *Tectonics*, **19,** 1095–1106.
Jolivet, L., Goffé, B., Monié, P., Truffert-Luxey, C., Patriat, M. & Bonneau, M., 1996. Miocene detachment in Crete and exhumation P-T-t paths of high-pressure metamorphic rocks. *Tectonics*, **15,** 1129–1153.
Jolivet, L., Faccenna, C., Goffé, B., Burov, E.B. & Agard, P., 2003. Subduction tectonics and exhumation of high-pressure metamorphic rocks in the mediterranean orogens. *American Journal of Science*, **303,** 353–409.
Jolivet, L., Rimmelé, G., Oberhänsli, R., Goffé, B. & Candan, O., 2004. Correlation of syn-orogenic tectonic and metamorphic events in the Cyclades, the Lycian nappes and the Menderes massif. Geodynamic implications. *Bulletin De La Societe Geologique De France*, **175,** 217–238.
Jolivet, L., Faccenna, C., Huet, B. *et al*., 2013. Aegean tectonics: strain localisation, slab tearing and trench retreat. *Tectonophysics*. In press.
van der Kaaden, G., 1966. The significance and distribution of glaucophane rocks in Turkey. *Bulletin of the Mineral Research and Exploration Institute of Turkey*, **67,** 37–67.
Kadioğlu, Y.K., Dilek, Y., Güleç, N. & Foland, K.A., 2003. Tectonomagmatic evolution of bimodal plutons in the central Anatolian crystalline complex, Turkey. *Journal of Geology*, **111,** 671–690.
Ketin, I., 1966. Tectonic units of Anatolia. *Maden Tetkik ve Arama Bulletin*, **66,** 23–34.
Kocak, K. & Leake, B.E., 1994. The petrology of the Ortaköy district and its ophiolite at the western edge of the Middle Anatolian Massif, Turkey. *Journal of African Earth Sciences*, **18,** 163–174.
Lagos, M., Scherer, E.E., Tomaschek, F. *et al*., 2007. High precision lu-hf geochronology of eocene eclogite-facies rocks from syros, cyclades, Greece. *Chemical Geology*, **243,** 16–35.
Lanari, P., Guillot, S., Schwartz, S. *et al*., 2012a. Diachronous evolution of the alpine continental subduction wedge: Evidence from P-T estimates in the Brianconnais Zone houillere (France - Western Alps). *Journal of Geodynamics*, **56–57,** 39–54.
Lanari, P., Vidal, O., Schwartz, S., Riel, N., Guillot, S. & Lewin, E., 2012b. Deciphering P-T paths in metamorphic rocks involving zoned minerals using quantified maps (XMapTools software) and thermodynamics methods: examples from the Alps and the Himalaya. *Geophysical Research Abstracts*, **14,** 10605.
Lanari, P., Riel, N., Guillot, S. *et al*., 2013. Deciphering High-Pressure metamorphism in collisional context using microprobe-mapping methods: application to the Stak eclogitic massif (NW Himalaya). *Geology*, **41,** 111–114.
Lefebvre, C., Barnhoorn, A., van Hinsbergen, D.J.J., Kaymakcı, N. & Vissers, R.L.M., 2011. Late Cretaceous extensional denudation along a marble detachment fault zone in the Kırşehir massif near Kaman, central Turkey. *Journal of Structural Geology*, **33,** 1220–1236.
Liou, J.G., Zhang, R. & Ernst, W.G., 1994. An introduction to ultrahigh-pressure metamorphism. *The Island Arc*, **3,** 1–24.
Lips, A.L.W., Cassard, D., Sözbilir, H., Yılmaz, H. & Wijbrans, J.R., 2001. Multistage exhumation of the Menderes Massif, western Anatolia (Turkey). *International Journal of Earth Sciences*, **89,** 781–792.
Malinverno, A. & Ryan, W.B.F., 1986. Extension in the Tyrrhenian Sea and shortening in the Apennines as result of arc migration driven by sinking of the lithosphere. *Tectonics*, **5,** 227–245.
McDougall, I. & Harrison, T.M., 1999. *Geochronology and Thermochronology by the 40Ar/39Ar Method*. Oxford University Press, New York, Oxford.
Monod, O., Kozlu, H., Ghienne, J.F. *et al*., 2003. Late Ordovician glaciation in southern Turkey. *Terra Nova*, **15,** 249–257.
MTA, 2002. *Geological Map of Turkey, 1:500,000*. MTA, Ankara.
Oberhänsli, R., Monié, P., Candan, O., Warkus, F.C., Partzsch, J.H. & Dora, O.Ö., 1998. The age of blueschist metamorphism in the Mesozoic cover series of the Menderes Massif. *Schweizerische Mineralogische Und Petrographische Mitteilungen*, **78,** 309–316.
Oberhänsli, R., Partzsch, J., Candan, O. & Cetinkaplan, M., 2001. First occurrence of Fe-Mg-carpholite documenting a high-pressure metamorphism in metasediments of the Lycian Nappes, SW Turkey. *International Journal of Earth Sciences*, **89,** 867–873.
Oberhänsli, R., Bousquet, R., Candan, O. & Okay, A., 2012. Dating subduction events in East Anatolia, Turkey. *Turkish Journal of Earth Sciences*, **21,** 1–17.
Okay, A.I., 1984. Distribution and characteristics of the northwest Turkish blueschists. In: *The Geological Evolution of the Eastern Mediterranean*, Vol. **17** (eds Dixon, J.E. & Robertson,

A.H.F.), pp. 455–466. *Geological Society, London, Special Publications*.
Okay, A.I., 2001. Stratigraphic and metamorphic inversions in the central Menderes Massif: a new structural model. *International Journal of Earth Sciences*, **89,** 709–727.
Okay, A.I., 2002. Jadeite-chloritoid-glaucophane-lawsonite blueschists in northwest Turkey: unusually high P/T ratios in continental crust. *Journal of Metamorphic Geology*, **20,** 757–768.
Okay, A.I. & Kelley, S.P., 1994. Tectonic Setting, Petrology and Geochronology of Jadeite Plus Glaucophane and Chloritoid Plus Glaucophane Schists from North-West Turkey. *Journal of Metamorphic Geology*, **12,** 455–466.
Okay, A.I. & Sahinturk, O., 1997. Geology of the Eastern Pontides. In: *Regional and Petroleum Geology of the Black Sea and Surrounding Region*, Vol. **68** (ed. Robinson, A.G.), pp. 291–311, AAPG Memoir, Tulsa, OK.
Okay, A.I. & Satır, M., 2006. Geochronology of Eocene plutonism and metamorphism in northwest Turkey: evidence for a possible magmatic arc. *Geodinamica Acta*, **19,** 251–266.
Okay, A.I. & Tüysüz, O., 1999. Tethyan sutures of northern Turkey. In: *The Mediterranean Basins: Tertiary Extension within the Alpine Orogen*, Vol. **156** (eds Durand, B., Jolivet, L., Horváth, F. & Séranne, M.), pp. 475–515. *Geological Society, London, Special Publications*.
Okay, A.I., Satır, M., Maluski, H. *et al*., 1996. Paleo- and Neo-Tethyan events in northwestern Turkey: geologic and geochronologic constraints. In: *The Tectonic Evolution of Asia* (eds Yin, A. & Harrison, T.M.), pp. 420–441. University Press, Cambridge.
Okay, A.I., Harris, N.B.W. & Kelley, S.P., 1998. Exhumation of blueschists along a Tethyan suture in northwest Turkey. *Tectonophysics*, **285,** 275–299.
Okay, A.I., Tansel, I. & Tüysüz, O., 2001. Obduction, subduction and collision as reflected in the Upper Cretaceous-Lower Eocene sedimentary record of western Turkey. *Geological Magazine*, **138,** 117–142.
Önen, A.P. & Hall, R., 1993. Ophiolites and related metamorphic rocks from the Kütahya region, North-West Turkey. *Geological Journal*, **28,** 399–412.
Özcan, A., Göncüoğlu, M., Turan, N., Uysal, Ş., Senturk, K. & Işık, V., 1988. Late Paleozoic Evolution of the Kütahya-Bolkardağ Belt. *METU Journal of Pure and Applied Sciences*, **21,** 211–220.
Özer, S. & Tansel Öngen, I., 2012. Correlation of the Upper Cretaceous sequences between Afyon Zone and Menderes Massif based on the new palaeontologic data (rudist and planktic foraminifera). In: 65th Geological Congress of Turkey, Ankara, Turkey.
Özer, S., Sözbilir, H., Özkar, I., Toker, V. & Sari, B., 2001. Stratigraphy of Upper Cretaceous-Palaeogene sequences in the southern and eastern Menderes Massif (western Turkey). *International Journal of Earth Sciences*, **89,** 852–866.
Papanikolaou, D., 2009. Timing of tectonic emplacement of the ophiolites and terrane paleogeography in the Hellenides. *Lithos*, **108,** 262–280.
Parlak, O. & Delaloye, M., 1999. Precise ^{40}Ar-^{39}Ar ages from the metamorphic sole of the Mersin ophiolite (southern Turkey). *Tectonophysics*, **301,** 145–158.
Parlak, O., Delaloye, M. & Bingol, E., 1996. Mineral chemistry of ultramafic and mafic cumulates an indicator of the arc-related origin of Mersin ophiolite (southern Turkey). *Geologische Rundschau*, **85,** 647–661.
Parra, T., Vidal, O. & Agard, P., 2002. A thermodynamic model for Fe-Mg dioctahedral K white micas using data from phase-equilibrium experiments and natural pelitic assemblages. *Contributions to Mineralogy and Petrology*, **143,** 706–732.
Pourteau, A., 2011. Closure of the Neotethys Ocean in Anatolia: structural, petrologic & geochronologic insights from low-grade high-pressure metasediments, Afyon Zone. PhD thesis, Universität Potsdam, Potsdam.
Pourteau, A., Candan, O. & Oberhänsli, R., 2010. High-Pressure metasediments in central Turkey: constraints on the Neotethyan closure history. *Tectonics*, **29,** TC5004.
Reddy, S.M., Kelley, S.P. & Wheeler, J., 1996. A ^{40}Ar/^{39}Ar laser probe study of micas from the Sesia Zone, Italian Alps: implications for metamorphic and deformation histories. *Journal of Metamorphic Geology*, **14,** 493–508.
Régnier, J.L., Ring, U., Passchier, C.W., Gessner, K. & Güngör, T., 2003. Contrasting metamorphic evolution of metasedimentary rocks from the Cine and Selimiye nappes in the Anatolide belt, western Turkey. *Journal of Metamorphic Geology*, **21,** 699–721.
Rimmelé, G., Jolivet, L., Oberhänsli, R. & Goffé, B., 2003a. Deformation history of the high-pressure Lycian Nappes and implications for tectonic evolution of SW Turkey. *Tectonics*, **22,** 1007.
Rimmelé, G., Oberhänsli, R., Goffé, B., Jolivet, L., Candan, O. & Çetinkaplan, M., 2003b. First evidence of high-pressure metamorphism in the "Cover Series" of the southern Menderes Massif. Tectonic and metamorphic implications for the evolution of SW Turkey. *Lithos*, **71,** 19–46.
Rimmelé, G., Parra, T., Goffé, B., Oberhänsli, R., Jolivet, L. & Candan, O., 2005. Exhumation paths of high-pressure-low-temperature metamorphic rocks from the Lycian Nappes and the Menderes Massif (SW Turkey): a multi-equilibrium approach. *Journal of Petrology*, **46,** 641–669.
Rimmelé, G., Oberhänsli, R., Candan, O., Goffé, B. & Jolivet, L., 2006. The wide distribution of HP-LT rocks in the Lycian Belt (Western Turkey): implications for accretionary wedge geometry In: *Tectonic Development of the Eastern Mediterranean Region*, Vol. **260** (eds Robertson, A.H.F. & Mountrakis, D.), pp. 447–466. *Geological Society, London, Special Publications*.
Ring, U. & Layer, P.W., 2003. High-pressure metamorphism in the Aegean, eastern Mediterranean: underplating and exhumation from the Late Cretaceous until the Miocene to Recent above the retreating Hellenic subduction zone. *Tectonics*, **22,** 1022.
Ring, U., Gessner, K., Güngör, T. & Passchier, C.W., 1999. The Menderes Massif of western Turkey and the Cycladic Massif in the Aegean - do they really correlate? *Journal of the Geological Society, London*, **156,** 3–6.
Ring, U., Willner, A.P. & Lackmann, W., 2001. Stacking of nappes with different pressure-temperature paths: an example from the Menderes nappes of western Turkey. *American Journal of Science*, **301,** 912–944.
Ring, U., Will, T., Glodny, J. *et al*., 2007. Early exhumation of high-pressure rocks in extrusion wedges: CYCLADIC blueschist unit in the eastern Aegean, Greece, and Turkey *Tectonics*, **26,** TC2001.
Ring, U., Glodny, J., Will, T. & Thomson, S., 2010. The Hellenic Subduction System: high-Pressure Metamorphism, Exhumation, Normal Faulting, and Large-Scale Extension. *Annual Review of Earth and Planetary Sciences*, **38,** 45–76.
Robertson, A.H.F., 2002. Overview of the genesis and emplacement of Mesozoic ophiolites in the Eastern Mediterranean Tethyan region. *Lithos*, **65,** 1–67.
Rolland, Y., Billo, S., Corsini, M., Sosson, M. & Galoyan, G., 2009. Blueschists of the Amassia-Stepanavan Suture Zone (Armenia): linking Tethys subduction history from E-Turkey to W-Iran. *International Journal of Earth Sciences*, **98,** 533–550.
Royden, L. & Burchfiel, B.C., 1989. Are systematic variations in thrust belt style related to plate boundary processes? (the Western Alps versus the Carpathians). *Tectonics*, **8,** 51–61.
Salaün, G., Pedersen, H.A., Paul, A. *et al*., 2012. High-resolution surface wave tomography beneath the Aegean-Anatolia region: constraints on upper-mantle structure. *Geophysical Journal International*, **190,** 406–420.
Saporta, G., 1990. *Probabilités, analyse des données et statistique*, Editions Technip, Paris.

Satır, M. & Friedrichsen, H., 1986. The origin and evolution of the Menderes Massif, W-Turkey: a rubidium/strontium and oxygen isotope study. *Geologische Rundschau*, **75,** 703–714.
Schellart, W.P., 2010. Evolution of Subduction Zone Curvature and its Dependence on the Trench Velocity and the Slab to Upper Mantle Viscosity Ratio. *Journal of Geophysical Research-Solid Earth*, **115,** B11406.
Schmid, S.M., Fugenschuh, B., Kissling, E. & Schuster, R., 2004. Tectonic map and overall architecture of the Alpine orogen. *Eclogae Geologicae Helvetiae*, **97,** 93–117.
Schuiling, R.D., 1962. On petrology, age and structure of the Menderes migmatite complex (SW-Turkey). *Bulletin of the Mineral Research and Exploration Institute of Turkey*, **58,** 71–84.
Seaton, N.C.A., Whitney, D.L., Teyssier, C., Toraman, E. & Heizler, M.T., 2009. Recrystallization of high-pressure marble (Sivrihisar, Turkey). *Tectonophysics*, **479,** 241–253.
Şengör, A.M.C. & Yılmaz, Y., 1981. Tethyan Evolution of Turkey – a Plate Tectonic Approach. *Tectonophysics*, **75,** 181–241.
Şengör, A.M.C., Satır, M. & Akkok, R., 1984. Timing of tectonic events in the Menderes Massif, Western Turkey – Implications for tectonic evolution and evidence for Pan-African basement in Turkey. *Tectonics*, **3,** 693–707.
Seymen, I., 1981. Stratigraphy and metamorphism of the Kırşehir Massif around Kaman (Kırşehir - Turkey). *Bulletin of the Geological Society of Turkey*, **24,** 7–14.
Sherlock, S. & Kelley, S., 2002. Excess argon evolution in HP-LT rocks: a UVLAMP study of phengite and K-free minerals, NW Turkey. *Chemical Geology*, **182,** 619–636.
Sherlock, S., Kelley, S., Inger, S., Harris, N.B.W. & Okay, A.I., 1999. Ar-40-Ar-39 and Rb-Sr geochronology of high-pressure metamorphism and exhumation history of the Tavsanli Zone, NW Turkey. *Contributions to Mineralogy and Petrology*, **137,** 46–58.
de Sigoyer, J., Chavagnac, V., Blichert-Toft, J. *et al*., 2000. Dating the Indian continental subduction and collisional thickening in the northwest Himalaya: multichronology of the Tso Morari eclogites. *Geology*, **28,** 487–490.
Spakman, W. & Hall, R., 2010. Surface deformation and slab-mantle interaction during Banda arc subduction rollback. *Nature Geoscience*, **3,** 562–566.
Theye, T., Seidel, E. & Vidal, O., 1992. Carpholite, sudoite and chloritoid in low-grade high-pressure metapelites from Crete and the Peloponnese, Greece. *European Journal of Mineralogy*, **4,** 487–507.
Trotet, F., Jolivet, L. & Vidal, O., 2001. Tectono-metamorphic evolution of Syros and Sifnos islands (Cyclades, Greece). *Tectonophysics*, **338,** 179–206.
Trotet, F., Goffé, B., Vidal, O. & Jolivet, L., 2006. Evidence of retrograde Mg-carpholite in the Phyllite-Quartzite nappe of Peloponnese from thermobarometric modelisation - geodynamic implications. *Geodynamica Acta*, **19,** 323–343.
Vidal, O. & Parra, T., 2000. Exhumation paths of high pressure metapelites obtained from local equilibria for chlorite-phengite assemblages. *Geological Journal*, **35,** 139–161.
Vidal, O., Parra, T. & Trotet, F., 2001. A thermodynamic model for Fe-Mg aluminous chlorite using data from phase equilibrium experiments and natural pelitic assemblages in the 100–600°C, 1–25 kbar range. *American Journal of Science*, **301,** 557–592.
Vidal, O., Parra, T. & Vieillard, P., 2005. Thermodynamic properties of the Tschermak solid solution in Fe-chlorite: application to natural examples and possible role of oxidation. *American Mineralogist*, **90,** 347–358.
Vidal, O., De Andrade, V., Lewin, E., Munoz, M., Parra, T. & Pascarelli, S., 2006. P-T-deformation-$Fe3^+/Fe2^+$ mapping at the thin section scale and comparison with XANES mapping: application to a garnet-bearing metapelite from the Sambagawa metamorphic belt (Japan). *Journal of Metamorphic Geology*, **24,** 669–683.
Whitney, D.L., 2002. Coexisting andalusite, kyanite, and sillimanite: sequential formation of three Al_2SiO_5 polymorphs during progressive metamorphism near the triple point, Sivrihisar, Turkey. *American Mineralogist*, **87,** 405–416.
Whitney, D.L. & Bozkurt, E., 2002. Metamorphic history of the southern Menderes massif, western Turkey. *Geological Society of America Bulletin*, **114,** 829–838.
Whitney, D.L. & Davis, P.B., 2006. Why is lawsonite eclogite so rare? Metamorphism and preservation of lawsonite eclogite, Sivrihisar, Turkey. *Geology*, **34,** 473–476.
Whitney, D.L. & Evans, B.W., 2010. Abbreviations for names of rock-forming minerals. *American Mineralogist*, **95,** 185–187.
Whitney, D.L., Teyssier, C., Dilek, Y. & Fayon, A.K., 2001. Metamorphism of the Central Anatolian Crystalline Complex, Turkey: influence of orogen-normal collision vs, wrench-dominated tectonics on *P-T-t* paths. *Journal of Metamorphic Geology*, **19,** 411–432.
Whitney, D.L., Teyssier, C., Fayon, A.K., Hamilton, M.A. & Heizler, M., 2003. Tectonic controls on metamorphism, partial melting, and intrusion: timing and duration of regional metamorphism and magmatism in the Nigde Massif, Turkey. *Tectonophysics*, **376,** 37–60.
Whitney, D.L., Teyssier, C. & Heizler, M.T., 2007. Gneiss domes, metamorphic core complexes, and wrench zones: thermal and structural evolution of the Nigde Massif, central Anatolia, *Tectonics*, **26,** TC5002.
Whitney, D.L., Teyssier, C., Kruckenberg, S.C., Morgan, V.L. & Iredale, L.J., 2008. High-pressure-low-temperature metamorphism of metasedimentary rocks, southern Menderes Massif, western Turkey. *Lithos*, **101,** 218–232.
Whitney, D.L., Teyssier, C., Toraman, E., Seaton, N.C.A. & Fayon, A.K., 2011. Metamorphic and tectonic evolution of a structurally continuous blueschist-to-Barrovian terrane, Sivrihisar Massif, Turkey. *Journal of Metamorphic Geology*, **29,** 193–212.
Wiederkehr, M., Sudo, M., Bousquet, R., Berger, A. & Schmid, S.M., 2009. Alpine orogenic evolution from subduction to collisional thermal overprint: the (40)Ar/(39)Ar age constraints from the Valaisan Ocean, central Alps. *Tectonics* **28,** TC6009.
Wijbrans, J.R. & McDougall, I., 1986. $^{40}Ar/^{39}Ar$ Dating of White Micas from an Alpine High-Pressure Metamorphic Belt on Naxos (Greece) - the Resetting of the Argon Isotopic System. *Contributions to Mineralogy and Petrology*, **93,** 187–194.
Yılmaz, Y., Genç, S.C., Yiğitbaş, E., Bozcu, M. & Yılmaz, K., 1995. Geological Evolution of the Late Mesozoic Continental-Margin of Northwestern Anatolia. *Tectonophysics*, **243,** 155–171.
Yılmaz, Y., Genç, S.C., Gürer, F. *et al*., 2000. When did the western Anatolian grabens begin to develop? In: *Tectonics and Magmatism in Turkey and the Surrounding Area*, Vol. **173** (eds Bozkurt, E., Winchester, J.A. & Piper, J.D.A.), pp. 353–384. *Geological Society, London, Special Publications*.

SUPPORTING INFORMATION

Additional Supporting Information may be found in the online version of this article at the publisher's web site:

Appendix S1. Ar isotope analytical procedure.

Table S1. Coordinates and mineral assemblages of the study samples.

Table S2. Correction factors for interference of Ar isotopes derived from K and Ca.

Table S3. $^{40}Ar–^{39}Ar$ geochronology data.

Received 20 September 2011; revision accepted 7 March 2013.